Collège de France LPC/94-48
28/11/94

Développement de compteurs Cerenkov à image annulaire pour l'identification des particules

T. Ypsilantis et J. Seguinot
Collège de France, Paris

Résumé

On présente les principes des compteurs Cerenkov à image annulaire pour l'identification des particules en physique des hautes énergies avec une discussion sur leur domaine d'application et une comparaison avec d'autres méthodes de détermination de la vitesse.

L'utilisation de la photo-ionisation en phase gazeuse pour la détection de photons Cerenkov UV uniques a conduit à une large gamme de détecteurs à image annulaire. On fait la revue du développement dans les dix sept dernières années, des différents types de détecteurs, de leur fonctionnement et de leur application à des expériences données.

On présente la possibilité d'utiliser les détecteurs à image annulaire pour la détermination simultanée de la vitesse et de l'impulsion dans des configurations géométriques spéciales de compteurs.

Présenté par T. Ypsilantis à la Conférence d'ERICE : " History of Original Ideas and Basic Discoveries in Particle Physics". 29/7-8/4/94.

Collège de France LPC/94-48
28/11/94

Development of Ring Imaging Cherenkov Counters for Particle Identification

T. Ypsilantis and J. Seguinot
Collège de France, Paris

Abstract

The principles of Cherenkov ring imaging for particle identification in High Energy Physics are presented with a discussion of their domain of application and comparison with other methods of velocity determination.

The use of gas phase photoionization for detection of single UV Cherenkov photons has led to a broad range of ring imaging detectors. The development over the past 17 years of the different detectors types, their performance and their application in specific experiments is recounted.

The possible use of ring imaging detectors for both velocity and momentum determination in specific counter geometries is presented.

KEYWORDS: Cherenkov counters.

Presented by T. Ypsilantis at the Erice Conference on " History of Original Ideas and Basic Discoveries in Particle Physics". 29/7-8/4/94.

1. Cherenkov Radiation

1.1 Discovery and Confirmation

Observation by Mme. Curie in 1910 of blue light emitted from concentrated radium solutions long preceeded elucidation of this effect. The first quantative observations, visual and photographic, by Mallet [1] between 1926 and 1929 showed that the spectrum was continuous whereas fluorescence, which was extensively studied during this same period, exhibited discrete spectral lines.

The exhaustive experiments of Cherenkov between 1934 and 1944 characterized this radiation [2] for which he, with Frank and Tamm, was awarded the Nobel Prize in 1958. This work is remarkable by its directness and simplicity. With rather rudimentary detectors (film) and sources (β-rays or Compton electrons) he measured the angular distribution of the radiation, its spectral distribution, its total intensity and its dependance on n and β. He demonstrated, in addition, that the light intensity was proportional to the electron path length and that the radiation was polarized and fast. Measurements with both hard and soft γ-rays showed a threshold effect and the radiation was found to be identical when excited by either β or γ-rays.

These data preceeded and are fully consistent with the classical electromagnetic theory of this effect developed by Frank and Tamm [3] in 1937. A quantum calculation by Ginsburg [4] in 1940 resulted in only minor modifications of the Frank-Tamm theory.

Experimental verification followed soon thereafter-by Collins and Reiling [5] in 1938 and by Wyckoff and Henderson [6] in 1943.

1.2 Cherenkov Angle and Intensity

A charged particle moving in an optical medium of refractive index n with velocity $v=c\beta$ will emit Cherenkov radiation if v exceeds the velocity of light in the medium (i.e $v > c/n$ or $\beta > 1/n$). The polar emission angle θ relative to the particle direction is given by the Cherenkov equation

$$\cos\theta = \frac{1}{n\beta} \tag{1}$$

whereas, the azimuthal emission angle φ has a flat distribution between 0 and 2π. The intensity and spectrum of the radiation is given by the Frank-Tamm relation

$$\frac{dN_{ph}}{dE} = \left(\frac{\alpha}{\hbar c}\right) Z^2 L \sin^2\theta \tag{2}$$

where dN_{ph} is the number of photons with energy between E and E+dE, α the electromagnetic fine structure constant, L the particle path length in the medium and Ze the charge of the particle. Combining, we obtain the (β, n) spectral dependance

$$\frac{dNph}{dE} = \left(\frac{\alpha}{\hbar c}\right) Z^2 L\left[1-(1/n\beta)^2\right] \tag{3}$$

The dispersion of an optical medium is expressed by a function n=n(E). The number of detected photoelectrons N is obtained by integrating over an energy bandwidth ΔE which, for constant Cherenkov angle (i.e. constant $n\beta$), gives

$$N = N_0 Z^2 L \sin^2\theta \tag{4}$$

where N_0 is the detector response parameter i.e.

$$\begin{aligned} N_0 &= (\alpha/\hbar c)\varepsilon\Delta E = \left(\frac{370}{eV-cm}\right)\varepsilon\Delta E \\ \varepsilon\Delta E &= \int (QTR)dE \end{aligned} \tag{5}$$

and ε is the energy average of detector efficiencies (Q=quantum, T=transmission, R=mirror reflection) between bottom E_b and top

$E_t=E_b+\Delta E$ energy limits. The spectrum is flat for constant n but, for real media both n(E) and dN_{ph}/dE increase with E.

A visible light photon detector e.g. a glass window photomultiplier (PM) has typically Q=0.2 at the first dynode, E_b=2 eV, E_t=3.2 eV thus ΔE=1.2 eV, which with R=0.9 and T=1 gives $\varepsilon\Delta E$=.216 eV and N_0=80/cm. Photoionization gas detectors, operating in the UV, have achieved comparible values of N_0 for about the same bandwidth ΔE but for R=T=0.8.

1.3 Threshold Counters

Threshold counters are preferred as detectors of secondary particles coming from an interaction region because their large phase space acceptance matches the emittance of the secondaries. Often, but not always, a threshold measurement ($\beta>\beta_t$) suffices to identify a particle if its momentum is measured by magnetic deflection. The threshold counter, placed before or after the magnet, has an elliptical mirror with foci positioned to be at the particle source and the PM detector. The radiator is made sufficiently long to obtain efficient detection of above threshold particles. Focusing with an elliptical mirror is possible because the gas Cherenkov angle is small (the optics assumes it zero).

For example, the tagged photon spectrometer experiment E691 at Fermilab of Bartlett et al. [7] had two large threshold counters C1 and C2 which attained N_0's of 70/cm and 123/cm respectively, with N≈15 in each counter. Even though N was large, ΔE was also large (5.3 eV) and ε was only 3.6% and 6.3%, respectively whereas, 18% could be expected from Eq. 5. The resolution σ_β/β is obtained from the variance of N (Eq. 4) as

$$\frac{\sigma_N}{N}=\frac{1}{\sqrt{N}}=2\cot\theta\sigma_\theta \qquad (6)$$

but from Eq. 1

$$\sigma_\theta = \cot\theta\left(\sigma_\beta/\beta\right) \tag{7}$$

hence

$$\frac{\sigma_\beta}{\beta} = \frac{\tan^2\theta}{2\sqrt{N}} \tag{8}$$

which, for C1 and C2 gives $\sigma_\beta/\beta=7.7\cdot10^{-5}$ and $2.3\cdot10^{-5}$, respectively. These counters had sufficient particle ID capability to reconstruct charmed particle masses in diverse decay modes [7]. In fact, the C2 resolution was only a factor 6 worse than the best chromatically corrected differential counter but, with the enormous advantage of large phase space acceptance. Their long lengths (3.8 m and 6.6 m), however, are not suited to colliding beam experiments but quite acceptable for fixed target spectrometers.

2. Ring Imaging Cherenkov Counters

This focusing method combines the good phase space acceptance of threshold counters with the superior β resolution of differential counters. In its original form, proposed by Roberts [8] in 1960 and shown in Fig. 1, it had a focusing lens which produced a Cherenkov ring on the surface of an image intensifier. The radius of the ring could be variable (not defined by slits) because of the uniform area sensitivity of the intensifier. Its angular acceptance was limited only by the intensifier area and lens size. The intensifier had a 2D imaging capability hence rings of any radius could be observed, however, in actual practice its small surface area, its low quantum efficiency and its low single electron sensitivity severely restricted this development.

The first ring images, obtained by Poultney et al. [9] in 1962, had N=4-6 but small N_0=2/cm. The better optical system of Binnie et al. [10] gave N=4 and N_0=12/cm whereas Iredale et al. [11] got N up to 25 but small $N_0\approx1.5$/cm. Finally, Giese et al. [12] got N=1.7

for a 9 m long radiator and N_0=15/cm. All these devices suffered from the small area and low efficiency of the intensifiers and no practical detectors emerged from this work.

The first practical Ring Imaging Cherenkov (RICH) detector was proposed and demonstrated by the Seguinot and Ypsilantis [13] in 1977. They showed that gas phase photoionization of selected molecules by UV Cherenkov photons could replace the PM as photosensor. Specifically, an admixture of Benzene with Argon gas in a multiwire chamber (MWC) allowed efficient single photon detection when one cathode of the MWC was replaced by a wire mesh and UV transparent window. The position sensitivity of a MWC allowed single pe's to be imaged and, because it can operate at atmospheric pressure, large areas can be covered near the mirror focal plane.

2.1 Angular Resolution and Particle Identification

The resolution σ_β/β of a RICH detector, given by Eq. 7 for a single pe, becomes for N pe's

$$\frac{\sigma_\beta}{\beta} = \tan\theta \frac{\sigma_\theta}{\sqrt{N}} \tag{9}$$

where σ_θ is the angular error per photon. This differs from Eq. 8 by the ratio $\tan\theta/(2\sigma_\theta)$ because RICH measures θ directly whereas a threshold counter only infers it from N. This factor can be as large as 250 for the least chromatic UV radiators (He or Ne at <E>=6.5 eV with ΔE=1 eV) and even larger for the visible region. A major additional advantage of RICH is that the Cherenkov angle θ is Gaussian distributed whereas dE/dx devices have Landau tails.

The particle ID capability of RICH is obtained by considering $u=\sin^2\theta$ which, from Eq. 1, may be written as

$$u = 1 - (1/n)^2 - (m/np)^2 \tag{10}$$

where p and m are particle momentum and mass. The number of standard deviations n_σ to discriminate mass m_2 from m_1 is then obtained from Eq. 10 as

$$n_\sigma = \frac{u_2 - u_1}{\left(\sigma_u/\sqrt{N}\right)} = \frac{m_2^2 - m_1^2}{p^2 n^2}\left(\frac{\sqrt{N}}{\sigma_u}\right) \tag{11}$$

where σ_u is the error in u per pe and $\sigma_u/\sqrt{N}$ is the error for N pe's. Combining Eq.s 4 and 9 with $\sigma_u=(2\sin\theta\cos\theta)\sigma_\theta=(2\sin\theta/n\beta)\sigma_\theta$ thus, particle ID with significance n_σ is attained at momentum

$$p = \sqrt{\frac{m_2^2 - m_1^2}{2k_r n_\sigma}} \tag{12}$$

where k_r is the RICH detector constant, defined as

$$k_r = \frac{n\beta\sigma_\theta}{\sqrt{N_0 L}} = \frac{\tan\theta\sigma_\theta}{\sqrt{N}} \tag{13}$$

The RICH resolution (Eq. 9) may now be rewritten as

$$\frac{\sigma_\beta}{\beta} = k_r \tag{14}$$

A 1.4 m long CF_4 gas radiator (1 bar, 20C) with detector response at $\langle E\rangle$=6.5 eV with ΔE=1 eV and N_0=75/cm has $k_r=1.6\cdot10^{-6}$, about 2.5 times better than the best chromatically corrected differential and 125 times better than the equivalent threshold counter (γ_t=31.8).

Comparison of RICH with time of flight (TOF) is obtained from the TOF equation $\beta ct=L$. The β resolution of TOF counter is

$$\sigma_\beta/\beta = \sigma_t/t_0 \tag{15}$$

where $t_0=L/\beta c$ and σ_t is the rms time resolution. Eq.'s 14, 15 show that RICH and TOF obey the same law (σ_β/β^2=constant) hence, equating constants, we get the equivalent time resolution of RICH $\sigma_t=t_0k_r$. The 1.4 m long CF_4 gas radiator has σ_t =9.3 fs, a factor 6400 times better than $\sigma_t\approx60$ ps measured in small scale TOF counters [14] and 13000 times better than $\sigma_t\approx120$ ps attained in large scale systems [15]. Obviously, TOF counters cannot compete with gas RICH counters in the high γ domain however, comparison should also be made in low γ domain where the Cherenkov radiators are necessarily liquid or solid. A RICH counter with a liquid C_6F_{14} radiator and focusing mirror can attain $k_r=3\cdot10^{-4}$ [16, 17] thus a TOF counter would need 1 ps time resolution over a 1 m flight path for same particle ID capability. A proximity focusing liquid RICH counter [17] has about 4 times worse resolution but this still corresponds to the excellent value σ_t=4 ps for L=1 m. Single photon timing with picosecond precision is far beyond present technological limits thus, the RICH technique is the only viable method for full particle ID, in the low as well as the high momentum range, up to ≈500 GeV/c (see Table 1).

If the particle mass is known, the ring image determines momentum $p=m\beta\gamma$. From Eq. 14 we get for the momentum error

$$\frac{\sigma_p}{p}=\gamma^2\frac{\sigma_\beta}{\beta}=\frac{k_r}{\beta^2}\left(\frac{p}{m}\right)^2 \tag{16}$$

For heavy particles (K,P), this error may be smaller than that from a magnetic deflection measurement.

2.2 Characteristic Optical Properties

The ring image optics is shown in Fig. 2 for two particles with zero impact parameter (relative to the mirror center of curvature). Here, the gas radiator fills the region between mirror and detector.

A spherical mirror of radius $r=r_m$ focuses a parallel bundle of Cherenkov light onto a point of the mirror focal plane $r=r_d=r_m/2$. The parallel rays contained in each of the two light bundles (shown in the plane of the figure) are focused at symmetric points about the particle track. Symmetry then requires that the image be a ring on the focal surface. In principal, many such images can be accomodated because different particles with direction (θ_p, φ_p) will have overlapping images only if they occupy the same point in the $(\beta, \theta_p, \varphi_p)$ space. However, the detector at the mirror focal plane must image single photons with good spatial resolution.

The previous argument shows that a ring image is centered about the particle track if the impact parameter $x_e=0$. However a parallel $x_e\neq0$ track forms an identical image since corresponding light bundles from each track are parallel so they must focus to the same point (aberrations only smear this point). Hence, the line between the ring and mirror centers gives the particle direction (θ_p, φ_p) and the ring radius (θ) gives the particle velocity β.

2.3 Measurement Errors

The measurements needed to define the Cherenkov angle θ are the photon detection point (z, x, y), the photon emission point (z_e, x_e) and particle direction (θ_p, φ_p). The photon emission point along the track is z_e and the impact parameter is x_e relative to the mirror center of curvature.

Six of these variables $(z, x, y, x_e, \theta_p, \varphi_p)$ can be arbitrarily well measured with errors depending only on the precision of the photon detector (z, x, y) and the tracker $(x_e, \theta_p, \varphi_p)$. However, the photon emission distance z_e has an error

$$\sigma_{z_e} = \Delta z_e/\sqrt{12} \tag{17}$$

which can be improved only by reducing the radiator path length $L=\Delta z_e$. The error in θ, for the variables $v_i=(z_e, x_e, z, x, y, \theta_p, \varphi_p)$, is

$$\sigma_\theta(v_i) = \left(\frac{\partial\theta}{\partial v_i}\right)\sigma_{v_i} \tag{18}$$

where $\partial\theta/\partial v_i$ is calculated from the reconstruction relation $\theta(v_i)$. The energy errors for square or triangular detector response are

$$\begin{aligned} \sigma_E &= \Delta E/\sqrt{12} \\ \sigma_E &= \Delta E/\sqrt{24} \end{aligned} \tag{19}$$

respectively. These can be improved only by reducing the energy bandwidth ΔE. The corresponding chromatic error is

$$\sigma_\theta(E) = \left(\frac{\partial\theta}{\partial n}\right)\left(\frac{dn}{dE}\right)\sigma_E \tag{20}$$

The errors (σ_{z_e}, σ_E) determine the irreducible resolution limits. Chromatic errors $\sigma_\theta(E)$ are discussed in § 2.4. The remaining errors $\sigma_\theta(v_i)$ require the function $\theta(v_i)$ which has been evaluated in [16, 17] for mirror and proximity focused optics.

2.4 Chromatic Errors

For a mirror focused image, the first factor of Eq. 20 is given by the derivative of Eq. 1 i.e

$$\frac{\partial\theta}{\partial n} = \frac{1}{n\tan\theta} = \left(\gamma_t - \gamma_t^{-1}\right)\Big/\sqrt{\left[1-(\gamma_\tau/\gamma)^2\right]} \tag{21}$$

written to exhibit its γ dependance and its asymptotic limit.
The second factor of Eq. 20 is the radiator dispersion which may be evaluated from the Lorentz-Lorenz equation

$$\frac{n^2-1}{n^2+2} = cf(E) \tag{22}$$

where $c=4\pi a^3\rho N_A/3M=(0.3738\ \mathrm{cm}^3)\rho/M$ with N_A Avagadro's number, a the Bohr radius, M the molecular weight and ρ the radiator density. The energy dependence of the molar refractivity f(E) is usually fit to a Sellmeir two-pole form

$$f(E)=\frac{F_1}{\left(E_1^2-E^2\right)}+\frac{F_2}{\left(E_2^2-E^2\right)} \tag{23}$$

The derivative of Eq. 22 then gives the dispersion

$$\frac{dn}{dE}=c\frac{\left(n^2+2\right)^2\frac{df}{dE}}{6n} \tag{24}$$

where n is from Eq. 22, c from molar density and df/dE is the derivative of Eq. 23. Sellmeir fits for radiator and window media are found in [17] and chromatic errors for gas radiators in Table 1.

2.5 Magnetic Field and Multiple Scattering Errors

Multiple scattering and magnetic deflection in the radiator medium represent additional error sources $\sigma_{\theta a}$ differing from the measurement and chromatic errors because they are momentum dependent. This error is written as $\sigma_{\theta a}=p_a/p$ where p_a has a value p_{ms} for multiple scattering (ms) or p_{ma} for magnetic field (ma) i.e

$$\begin{aligned} p_{ms} &= k_{ms}\sqrt{L/X_0} \\ p_{ma} &= k_{ma}BL\sin\theta_{ma} \end{aligned} \tag{25}$$

with resultant momentum $p_a=\sqrt{(p_{ms}^2+p_{ma}^2)}$. The constants are $k_{ms}=(2/3)(13.6)$ MeV=9.1 MeV, $k_{ma}=[(2/\pi)(.3)/\sqrt{12}]$ GeV/T-m=55.1 MeV/T-m where X_0 is the radiation length, B the magnetic field strength and θ_{ma} the particle angle relative to the magnetic field direction. The values of k_{ms} and k_{ma} are rms averages over the

path length L (the factor 2/3) and the image circumference (the factor $2/\pi$), respectively. Clearly, this error $\sigma_{\theta a}$ must be added in quadrature to the momentum independant error σ_θ. Defining a $q=p_a/(\sigma_\theta\sqrt{2})$ and $\sigma_\theta'=\sigma_\theta\sqrt{[1+2(q/p)^2]}$ then Eq. 12 has a new solution

$$p' = \sqrt{\left(p^4 + q^4\right)^{1/2} - q^2} \tag{26}$$

where p is the original solution of Eq. 12. As an example, suppose a gas counter has total error σ_θ=1 mrad, L=0.5 m, N_0=75/cm and $k_r=1.6\cdot10^{-5}$ hence $p=p_{\pi/K}(3\sigma)$=47.8 Gev/c (Eq. 12 for n_σ=3). With a magnetic field B=1.5 T at angle $\theta_{ma}=60^0$ then, p_{ma}=35.8 MeV, q=25.3 GeV and p'=39.4 GeV. Thus, $p_{\pi/K}(3\sigma)$ is reduced from 47.8 to 39.4 GeV because of the magnetic bend while radiating.

3. Detectors

We evaluate the merits of a detector system by an efficiency $\eta=N_0/N_0^c$, the ratio of the observed N_0 to that calculated from $N_0^c=(370\langle Q\rangle\Delta E)T_rT^nR^m$, where the integrated quantum efficiency is $\langle Q\rangle\Delta E=\int Q(E)dE$ with limits determined by the experimental conditions [18]. Each detector is characterized by n windows and m mirrors (default values n=m=1). The quantities, T_r, T and R are the energy averaged radiator, window transmissions and mirror reflectivity (default values 1, 0.75, 0.75, respectively). These factors are included in defining system efficiency because they, as well as the detector, must be optimized in order to get high performance. This is so because the number of Cherenkov photons is very small ($\approx$1 photon/10 keV of energy loss compared to $\approx$1 e/30 eV for ionization) thus, efficient use of each photon is essential. A more complete review of these detector developments is found in [18].

3.1 Multi-Step Avalanche Chambers

Here we consider Multi-Step Avalanche Chambers (MSACs) with a Pre-Amplification (PA) gap followed by a MWC (with fast

readout of wires) or a second PA gap (with slow readout of visible light or sparks). Except for our first tests with a MWC [13], all early results were obtained with MSACs [19].

The main goal of the first tests was simply to show that photoionization could actually be useful for Cherenkov imaging. Beam tests in 1978 by Durkin et al. [20] at SLAC and Gilmore et al. [21] at RAL with MWCs and Benzene gave the discouragingly low values $N_0 \approx 4.3/\mathrm{cm}$ while 82/cm is expected thus an efficiency of only 5%. Nevertheless, they showed that conventional MWCs with standard electronics could not efficiently detect single pe's.

In 1978 a new photosensitive gas triethylamine (TEA) became known. Its threshold of 7.5 eV is still somewhat high for chromatic aberrations but its large vapor pressure and short absorption length guaranteed 95% photon absorption in only 1.5 mm of gas pathlength at 20^0 C, hence fast response.

The first visual ring images were obtained by Charpak, Majewski, Melchart, Sauli and Ypsilantis [22] in late 1978 with the He+TEA filled hybrid MSAC (hybrid in the sense that a spark chamber followed the PA gap). Unambiguous 2D image points were obtained by viewing the sparks end-on with slow recording on film. An example of 30 superposed rings is shown in Fig. 3. An average of N=1.7 was detected from a 0.94 m long Ar gas radiator, thus $N_0 \approx 27/\mathrm{cm}$ compared to the expected $N_0^c = 78/\mathrm{cm}$ thus $\eta = 35\%$.

In 1979, Seguinot et al. [23] using an Ar gas radiator and a MSAC with gaps: C (conversion); PA; T (transfer) and PC (MWC), shown in Fig. 4, found for the maximum TEA quantum efficiency $Q_{max} = 37 \pm 6\%$ and $N_0 \approx 56/\mathrm{cm}$ thus $\eta = 72\%$ but now with fast electronic readout of 1D images. This result was confirmed and extended by Ekelof et al. [24] in 1980 using the same detector with total gain $\approx 10^6$ (PA$\leq 2 \cdot 10^3$, MWC$\leq 5 \cdot 10^4$) as shown in Fig. 5 (a), (b). Projected 1D rings, shown in Fig. 5 (c), were obtained by digital readout of anode wires. The data gave $Q_{max} = 34 \pm 4\%$ and $N_0 = 56/\mathrm{cm}$ thus $\eta = 72\%$ and showed that a PA+MWC with digital fast electronics could efficiently detect single pe's. Another major

result was to show that efficient (>95%) single pe counting was possible in a single gap MWC using CH_4 rather than Ar counting gas. On this basis, a long drift-time projection chamber (TPC) with a single electron sensitive MWC detector was proposed for unambiguous 2D imaging by electronic readout with TDCs.

A higher quantum efficiency for TEA (Q_{max}=46% at 8.4 eV) had been reported by the chemists Salomon and Scala [25] in 1975. Thus, the quantum response and spectral shape of TEA was remeasured by Holroyd et al. [26] in 1986 and Seguinot et al. [27] in 1988 with substantial agreement as shown in Fig. 6 and $Q_{max}\approx 32\%$.

The hybrid MSAC was improved in 1981 by Charpak et al. [28] with a fast TV camera for spark detection and CCD readout. It gave $N_0\approx 80$/cm thus efficiency η=103%. However, some secondary pe's were produced in the Ar gas (previous tests were in He) as shown by the photon pair-distance distribution.

The first use of RICH for particle ID was in experiment E605 at FNAL in 1981-83. An MSAC detector with TEA photosensor, CaF_2 windows and projective wire readout was built by a CERN-FNAL-Saclay-Stony Brook collaboration. It had a 16 m long NTP-He gas radiator (γ_t=118) with spherical mirrors (f=8 m) covering 6.7 m^2. Preliminary tests were made at 200 GeV/c with a 8 long STP-He gas radiator and f=8 m spherical mirror [29]. The MSAC had C, PA, T and MWC gaps filled with He+CH_4+TEA gas at NTP. Pseudo-2D image points were obtained with 0.37 mm rms accuracy by measuring with an ADC the centroid of the charge distribution induced on two orthogonal planes of cathode wire strips (2 mm pitch) oriented at $\pm 45^0$ to the anode wires, also with 2 mm pitch. The two photon resolution was 4-6 mm and, with 40 ns gating time, the detector was fast. The image points from 300 superimposed events, shown in Fig. 7 (a), are clean with little background. Three projective image planes (anode+2 cathodes) were read out and hits correlated by pulse height, as shown in Fig. 7 (b). The response of N_0=42/cm implies a good system efficiency η=79%, however, its angular resolution, σ_θ=59 μrad, is spectacular.

The He chromatic error is 43 μrad for TEA+CH_4 with triangular response from 7.5 to 9.3 eV (see Fig. 6). The quadrature difference of 40 μrad thus represents the pixel error i.e 0.32 mm in rough agreement with their quoted value of 0.37 mm. Fig. 7 (c) shows the excellent π/K particle ID attained at 200 GeV/c. For N_0=42/cm and σ_θ=59 μrad we find, from Eq. 12 for p=200 GeV/c, that n_σ=8.8 is expected and largely attained. The single event example of Fig. 7 (b) shows, however, that the multi-hit capability of this detector is limited to N≈4 because of its pseudo 2D nature of the readout. Notwithstanding, these tests showed the power of a RICH counter when coupled to a high efficiency, good spatial resolution detector.

Not much R&D was done on MSACs from 1984-87 as this period coincided with the main development period of the long drift-TPC. Since 1987, Breskin, Charpak, Sauli and others have investigated visible light emission during the avalanche process in MSACs filled with TEA or TMAE (see § 3.2). This technique has revived the optical readout method since it dispenses with the slow spark chamber but, because the emitted light intensity is small (≈1 photon/avalanche electron), two or more stages of image intensifier must preceed the CCD. First tests were made by Breskin et al. [30] in 1987 as R&D for the CERES experiment at CERN. The TMAE filled detector had stacked gaps C-PA-T-G-T-PA-LA (G for gating, LA for light amplification). It was operated at low pressure (40 torr of Ar+C_2H_6+TMAE) with a gating time of 2 μs, however the readout time of the CCD is much longer (≈10 ms). A response N_0=76/cm was attained for η=56% and an angular resolution σ_θ=1.3 mrad corresponding to $p_{\pi/K}(3\sigma)$=30 GeV/c.

3.2 Slow Drift Detectors with TPC Readout

Here we consider slow RICH detectors using long drift-TPC imaging with MWC or proportional tube detectors. In 1980, Anderson [31] introduced the new photosensitive molecule, Tetrakis-diMethyl-Amino-Ethylene (TMAE), with high quantum efficiency and a low threshold (5.3 eV) suitable for use with fused

quartz windows. We had previously shown that the long drift-TPC technique was advantageous for 2D (and even 3D) imaging of single electrons because it is simple, direct and unambiguous [24]. It allows large detector areas to be built at low cost because the number of electronic channels is minimized with the long drift-TPC technique, however it is slow. Moreover, TMAE allowed a much larger choice of solid, liquid and gas radiators with cheap, large area, fused quartz windows. The TMAE relative spectral response was first measured by the Japanese chemists Nakato et al. [32] in 1971. An absolute quantum efficiency Q vs λ was obtained by Ekelin [33] in 1981 and later by Holroyd et al. [26] and Seguinot et. al [27] as shown in Fig. 8. The data agree except that our value is 20% larger than Holroyd's in the important 6.2 to 7.2 eV region.

Thus, already in 1981, Barrelet et al. [34] worked with a 13 cm long drift-TPC-MWC detector with electronic readout of 2D images. Cherenkov photons entered the 13 cm long drift volume (DV) through a CaF_2 window. At the end of the DV, a single stage MWC was sited and each wire was readout by an 8-bit TDC. Initially, it was filled with TEA+CH_4 and excellent images were seen with N_0=33/cm and good efficiency η=83%.

Good images were also seen with a quartz windowed DV filled with CH_4+TMAE but now with significant (20%) photon feedback. The images (Fig. 9) display a snow background due to photon feedback, especially evident in this detector without blinds. The signal, after feedback subtraction, gave N_0=56/cm whereas 101/cm is expected thus, the efficiency degraded to η=56%. The observed angular resolution of σ_θ=2.2 mrad gives $p_{\pi/K}(3\sigma)\approx 36$ GeV/c for the 0.94 m long Ar gas radiator [35].

These results lead to development of the Ω-RICH by P. Sharp et al. [36] and DELPHI-RICH [37] both in 1982 and SLD-CRID by D. Leith et al. [38] in 1984. These three detectors, with more than 30 m^2 of photo-detector surface, are the largest in operation today.

The long drift results were confirmed by Dresselhaus and Fohrmann [39] in 1984. They used a N_2 gas radiator and a detector

similar to [34] but with (ethane, isobutane)+TMAE as filling gas. With isobutane they saw good images with N_0=68/cm and good efficiency η=84%. With ethane they found N_0=80/cm and η=63% thus showing the same degradation in efficiency as observed in going from TEA to TMAE. In both cases the number of feedback photons increased strongly: from ethane to isobutane because ethane is transparent to the 166 nm feedback line while isobutane is not; from TEA to TMAE because TEA is sensitive only to the 156 nm line while TMAE is sensitive to all three lines.

The production of secondary pe's became even more evident when, in 1982, Seguinot et. al. [40] tested the first proximity-focused liquid C_6F_{14} radiator. Earlier, they obtained and measured the transparency and refractive indices of the fluorocarbons CF_4, C_2F_6, C_4F_{10}, C_5F_{12} and C_6F_{14}, all in the liquid phase [27]. Good UV transparency was found with refractive indices $1.22 < n < 1.29$, as needed for particle ID at low momentum ($\leq$ 5 GeV/c). The detector and radiator are shown in Fig. 10. In the normal conditions of these tests, to get clean images without primary ionization effects, the beam passed between metallized plates. However, when the beam was displaced outside the plates, it produced, without TMAE, a small background but, with TMAE, the background became tremendously large. Hence, without some method to suppress feedback pe's, TMAE cannot be used with a single stage MWC. In this respect, MSACs are advantageous because, if the T gap between the two PA gaps is $>4 \cdot l_{abs}$, then feedback pe's will not be detected. With primary ionization suppressed and background subtracted, the events from 1 cm of liquid C_6F_{14} had N=18 pe's but bad angular resolution σ_θ=25 mrad, due to poor geometry i.e. (lever arm=4 cm, conversion depth=4.5 cm, radiator depth=1 cm). With better geometry, $\sigma_\theta \approx 10$ mrad could be expected. Nonetheless, this experiment showed that a proximity-focused liquid C_6F_{14} radiator produced good RICH images and was the experimental basis for the DELPHI-RICH proposal [37] and addendum [40].

A TPC-RICH counter with a gas radiator was used in 1984-85 by Bottner et al. [41] to measure prompt electron production in conjunction with the UA2 experiment at the CERN SppS collider.

3.2.1 DELPHI-RICH Prototype

Here we report the DELPHI-RICH Prototype project that we developed [42, 43, 44] as the first example of drift and detection of single electrons over 1.6 m. The geometry for π, K, P particle ID at LEP between 0.3 to 25 GeV/c is shown in Fig. 11. To cover this range we needed two Cherenkov radiators located on opposite sides of a common drift volume (DV) of 1.6 m length. On one side was a 1 cm thick proximity focused liquid C_6F_{14} radiator and on the other side was 50 cm of mirror focused gas C_5F_{12} radiator. The barrel structure consisted of 24 identical polygonal barrel staves (3 were built for the Prototype). Application of 100 kV at the central plane produced a uniform drift field $E_d \approx 0.6$ kV/cm with a maximum drift time of 25 μs. The now existing DELPHI Barrel RICH has a total DV surface of 27 m^2 per side with 14 K channels of 11 bit TDCs corresponding to 30 Mpixels, this large reduction factor being due to the long drift-TPC technique.

To eliminate parallax error, we obtained 3D point definition by readout (with 11 bit TDCs) of the MWC wires as well as crossed cathode strips. To minimize feedback, the detector was made of tubular cathodes around each anode wire of the MWC array. This structure had excellent gain stability with good suppression of feedback. The tube cathodes allowed high cathode strip detection efficiency at much lower gain thus significantly reducing feedback.

The first tests showed that E_d was constant within $\pm$ 0.3%, the transverse drift coefficient σ_{td}=179 μm/$\sqrt{\text{cm}}$ and the drift velocity v_d=6.3 cm/μs in 75%CH_4+25%C_2H_6+TMAE at E_d=0.58 kV/cm. Single pe's drifted 1.7 m with <15% loss thus l_{abs}>10 m [42, 43].

In Fig 12 are shown 100 superposed images from 10 GeV/c pions at normal incidence to the C_6F_{14} liquid radiator. The large ring is from the liquid, the small ring from the gas and the spot in

the center is from the beam. The liquid C_6F_{14} images at normal incidence had <N>=21 thus N_0=57/cm and η=89%. The gas images from the C_5F_{12} radiator had <N>=13 thus N_0=80/cm and η=100% [42]. Hence, the first results of the DELPHI Barrel RICH Prototype gave high detector efficiency and little photon feedback.

Images from the liquid radiator had resolution σ_θ=(12, 16) mrad for drift distances z=(0, 1.5) m. From the observed values <N>=21 and θ=679 mrad we have N_0=53/cm and η=83%. Hence $k_r=(2.1, 2.8)\cdot 10^{-3}$ and $p_{\pi/K}(3\sigma)$=(4.2, 3.6) GeV/c, respectively [44].

Gas radiator images had σ_θ=(4.5, 6) mrad for z=(0, 1.5) m. The observed values N=12 and θ=56 mrad gave N_0=77/cm, η=96%, $k_r=(7.2, 9.7)\cdot 10^{-5}$ and $p_{\pi/K}(3\sigma)$=(23, 20) GeV/c, respectively [44]..

The DELPHI-Prototype data may be summarized as: <η>=90% with angular resolutions and particle ID limits as expected. More important, the images were clean with little photon feedback.

3.2.2 The DELPHI-RICH

The first Barrel results were reported by Anassontzis et al. [45] and Baillon [46] in 1992. For Z^0s decaying into μ pairs they obtained liquid and gas N_0's of 32 and 50/cm and σ_θ's of 13.9 and 4.5 mrad respectively. However, for Z^0s decaying into hadronic jets an intrinsic liquid resolution σ_θ=17 mrad was observed as shown by the upper curve of Fig. 13. The background under the peak is larger than expected from jet multiplicity alone (10 particles above 0.5 GeV/c). Using a software cleaning method, a large part of this background can be removed-off line (lower curve of Fig. 13).

This background degrades σ_θ from 17 mrad observed to 23 mrad. The degradation in the gas radiator is from 7 mrad observed to 9 mrad [46]. These σ_θ's and the above N_0's give $p_{\pi/K}(3\sigma)$=2.5 and 13.6 GeV/c, respectively, consistent with the scatter plots of Fig. 14.

3.2.3 The SLD-CRID

The state of the SLD Cherenkov Ring Imaging Detector (CRID) was reported by Abe et al. [47] in 1993. They use blinded (2D)

MWCs with charge division to eliminate parallax. This method senses directly the charge on a wire rather than induced charge on a cathode strip thus, they dont require high gain in order to get good depth coordinate efficiency. Consequently, they obtain an average detector efficiency (η=75%) better than the DELPHI Barrel (η=57%) but not as good as the DELPHI Prototype (η=90%). It also appears that the feedback problem in SLD is less intense than the DELPHI Barrel, consistent with this hypothesis.

3.2.4 The Ω–RICH

The Ω-RICH detector was constructed by P. Sharp et al. [36] at CERN from 1982-1985 for a high energy photoproduction experiment WA69 at the Ω-Spectrometer facility. It has a 5 m long radiator filled with 120 m^3 of N_2 gas at atmospheric pressure. An array of 7 x 4 m^2 mirrors focuses the images onto 16 TPC chambers (80 x 40 cm^2) each with a quartz entrance window, as shown in Fig. 15. The detectors were blinded MWCs with a CH_4+C_4H_{10}+TMAE gas mixture. The first results published by Apsimon et. al. [48] in 1986 gave a rather low N_0=35/cm with 80/cm expected thus an efficiency η=44%. It showed, however, good angular resolution σ_θ=0.71 mrad thus allowing π/K separation to 83 GeV/c (3σ). This first version of Ω-RICH allowed the WA69 group to measure inclusive π and K photoproduction while the WA82 group identified various D-meson decay modes.

For a new hyperon beam experiment WA89, the Ω-RICH was subjected to an important upgrade in 1988-89 with results reported by Beusch et al. [49] in 1992. Five TPC units (1.6 x 0.75 m^2) were remade and the central part of the mirror array was replaced. The drift and TMAE carrier gas is now pure C_2H_6. The Cherenkov ring radius distribution for particles between 50 and 55 GeV/c is shown in Fig. 16. The N_0 now attained is 49/cm, better than before but still lower than N_0=127/cm expected thus, η=39%. The angular resolution σ_θ is 0.58 mrad intrinsic and 0.75 mrad with background. These numbers give $p_{\pi/K}(3\sigma)$=92 GeV/c, very near

their goal of 100 GeV/c. More details on performance, background and stability have been reported by Siebert et al. [50].

3.2.5 Astrophysics

Recently, Swordy et al. [51] have used long drift TPC-RICH detectors for research in astrophysics.

4. Fast-RICH

Here we consider Fast-RICH counters, shown schematically in Fig. 17, with pad readout and MSAC or MWC amplification. Since pad detectors are intrinsically 2D, they permit fast access to the physics in high multiplicity events however electronic readout speed is critical because of the large numbers of channels needed ($>10^5$ currently envisaged). We therefore consider that a Fast-RICH detector has fast gas amplification, fast readout electronics and can operate at hadron colliders with ≈40 MHz interaction rates with data readout at rates ≈100 kHz. This requires integrated electronics implanted on the detector to readout hit pads with minimum external connections. Pad detectors were first used by Coutrakon et al. in 1985 at FNAL [52] but with discrete readout electronics.

Fast operation requires small dispersion in electron arrival times ($\sigma_t \approx 10$ ns) thus a short absorption length. This is easily attained with TEA at 20C but would require TMAE heated to 100C.

Four groups have published R&D on pad photon detectors i.e. Coutrakon et al. [52] for E651 at Fermilab, Baur et al. [53, 54] for the CERES experiment at CERN and Braem et al. [55] for LHC heavy-ions at CERN and Arnold et al. [56] for B physics.

The R&D tests conducted by Breskin et al. [30] in 1987-88 used a low pressure (40 Torr) MSAC filled with C_2H_6+Ar +TMAE at 34C. The 200 x 200 mm^2 detector operated with C, PA, G, T gaps ending with a MWC. The central 84 x 84 mm^2 area was instrumented with pads of 2 mm diameter and 2.54 mm pitch. To reduce background, the G gap was opened only for 1 μs, the time needed

to accomodate the dispersion of the C gap. The 1089 pads were coupled to 9 Microplex chips each of 128 channels for analog readout at 100 kHz. Thus, neither the detector nor the readout satisfy the Fast-RICH criteria. A detector with a CaF_2 window was tested with images from a focused (f=1 m) CH_4 gas radiator at NTP. The N_0 measured was 102/cm whereas 135/cm is expected thus detector efficiency of 76%. The angular resolution of σ_θ=2.7 mrad was near the expected 2.5 mrad. In general, we prefer detectors which work at 1 bar and with MWC amplification for reasons safety and stability. In fact, the now existing CERES-RICH detector of Baur et al. [53] runs at 1 bar with PA-MWC amplification [54].

In 1988, a Fast-RICH detector with $4 \cdot 10^5$ pads was proposed for the symmetric e^+e^- B Meson Factory at PSI in Switzerland [56]. The accelerator project was not approved but development continued and may soon be used for other B-Factory projects. For this development, 2 years were spent on tests with small detectors working with pulsed UV light sources to investigate the response of pad detectors [56] before building the full scale prototype with 12000 pad channels as reported by Guyonnet et al. [57]. Equally important was the development at RAL of two ASICs for fast integrated readout of the pads as described by French et al. [58].

The Fast-RICH system proposed for the PSI-B-Factory covered 93% of 4π steradians with a NaF proximity focused radiator, a CaF_2 window and MWC detector and TEA photosensor. It would give $p_{\pi/K}(3\sigma)$=2.9 GeV/c, as needed for a symmetric e^+e^- B-Factory.

The Fast-RICH Prototype barrel is made of 3 polygonal barrel staves with $\Delta\varphi=12^0$ modularity with 0.9 m length and 20 cm of radial thickness comprising $\approx$15% X_0 with electronics. Each 12^0 sector is made of an asymmetric MWC fronting a pad arrays of 30 columns and 128 rows thus 3840 pads/sector. Pad sizes of 5.3 x 6.6 mm^2 were chosen to give a spatial resolution $\sigma_x=\sigma_y\approx$1 mm [56]. The 3 mm gas thickness of the MWC minimizes the ionization signal but still has good photon conversion efficiency and small pe

time dispersion ($\sigma_t \approx 10$ ns). The readout electronics is implanted on the backside of the detectors with short connections to the pads.

Development of the VLSI electronics took three iterations over about four years to obtain a viable product [58]. At the present time, 20K channels have been tested and are operative. This electronics allows digital pad hit data to be strobed in time intervals >20 ns into a 1.3 μs pipeline while waiting for an external readout trigger. Each sector is readout in parallel in about 2.5 μs.

Images with cosmic rays have been reported by Guyonnet et al. [57] along with details on the detector and electronics operation. We show here the data of Seguinot et al [59] from a later 10 GeV/c negative pion beam run with a 1 cm thick LiF crystal radiator. The scatter plot of hit pads (Fig. 18) shows clear and dense images. Two single events are shown in Fig. 19 with N=15 and 12 pe's, but the average $\langle N \rangle = 10.4$. The measured N_0 is 61/cm as compared to the expected value of 71/cm thus a good efficiency of $\eta = 86\%$. The distribution of reconstructed Cherenkov angles is shown in Fig. 20. The fit gives $\langle \theta \rangle = 835.5$ mrad and $\sigma_\theta = 13.8$ mrad with only a small background from the LiF scintillation. An analytical error calculation predicts $\sigma_\theta = 12.5$ mrad [17], not far from the 13.8 mrad observed. In general the images are very clean with negligible electronic noise. Each photon had 1.1 pad hits whereas the pion track had 2.3 but without any sign of photon feedback.

This device satisfies all criteria for a Fast-RICH however, it's resolution is limited by chromatic errors of the TEA photosensor.

5. Momentum and Mass from RICH for Long Baseline Neutrinos

The question of neutrino masses and mixing remains an important unsolved problem of particle physics. Experiments in this field use either accelerator neutrinos, solar neutrinos or atmospheric neutrinos, each sensitive to a different range of neutrino masses (m_ν) and mixing angles (α). The apparatus described here is conceived as a potential experiment for the Gran Sasso underground Laboratory, at a distance of 730 km from

CERN [60]. The possibility for such an experiment was already among the physics goals of the Gran Sasso Project [61] and special care was taken to build the experimental halls aligned towards CERN. The advantage of long baseline neutrino experiments is, of course, the increased sensitivity to small mass differences.

For such an experiment, the large RICH counter, shown schematically in Fig. 21, can serve simultaneously as target and detector. A cylindrical radiator, 20 m in diameter and 50 m in length, filled with Argon gas at (15 bar, 20 C, ρ=.025 g/cm^3) would contain 400 tons of sensitive target for neutrino interactions. The reflecting spherical mirror has a radius $r_m=R_M=100$ m and a photon detector on the mirror focal surface at radius $r=R_D=50.13$ m. The pixel size chosen is 30x30 mm^2 thus the detector has $3\cdot10^5$ channels (similar to B-Factory RICH detectors [56]). Several large area trackers are placed after the mirror to measure the direction of secondary charged particles and to determine the interaction vertex. This is followed by an iron filter and tracker to identify muons (another method is discussed below). A throughgoing $\beta=1$ charged particle in the gas radiator will produce $N\approx4000$ points on the ring image with a ring radius of 4.8 m and with good image quality even for the maximum impact parameter $x_e=10$ m. The chromatic error $\sigma_\theta(E)$ in Argon gas varies between 7 to 0.7 mrad whereas pixels of 30x30 mm^2 give errors $\sigma_\theta(x)=\sigma_\theta(y)=0.17$ mrad. Due to the unusually long (50 m) radiator, multiple scattering is not negligible and its contribution to the total error is dominant thus allowing particle ID (see below). Background should be small since the detector is directional and the beam is pulsed.

5.1 Signature for Neutrino Oscillations

The combination of a RICH counter and the external tracker will determine the charged particle momentum and direction. Direct muons ($\nu_\mu X\rightarrow\mu X'$) and indirect muons ($\nu_\tau X\rightarrow\tau X'$, $\tau\rightarrow\mu\nu_\tau$) may be identified on the basis of p and p_t measurements. For any initial neutrino energy, direct muons tend to have higher p (for a

given p_t) than do the indirect muons thus, cuts in the (p, p_t) plane can discriminate between the two processes.

5.2 Stereographic Projection of Cherenkov Rings

A neutrino interaction produces one or more above threshold charged particles ($\gamma > \gamma_t = 10$) which form circular images on the spherical detector surface. To display circles on spheres is difficult, we display instead a stereographic projection because a circle on a sphere is also a circle on the stereographic plane. Stereographically projected images of single CC events generated using PYTHIA 5.701 are shown in Fig. 22 for (a) a $\nu_\tau p$ event and (b) a $\nu_\mu p$ event.

5.3 Cherenkov Angle Reconstruction

A general method to reconstruct θ from the hit point (x, y, z) requires that the particle impact parameter x_e and the emission point z_e along the track be known [17]. From the tracker data, the interaction vertex (x_v, y_v, z_v) can be determined. The particle impact parameter is found from z_v, $\rho_v = \sqrt{(x_v^2 + y_v^2)}$ and θ_p as

$$x_e = z_v \sin\theta_p + \rho_v \cos\theta_p \tag{27}$$

assuming that all secondaries come from the same vertex. The photon emission point z_e cannot be measured thus, it is optimally assumed to be equidistant between z_v and $z_t = \sqrt{(r_m^2 - x_e^2)}$ i.e

$$z_e = \frac{z_v + \sqrt{r_m^2 - x_e^2}}{2} \tag{28}$$

Using these values of (x_e, z_e) and the photon hit points (x, y, z), we obtain the generalized detection angle Ω from the relation

$$\cos\Omega = \frac{(zz_e + xx_e)z_p + (xz_e - zx_e)x_p}{rr_e} \tag{29}$$

where $r_e=\sqrt{(x_e^2+z_e^2)}$, $z_p=\cos\theta_p$ and $x_p=\sin\theta_p$. We then find the generalized emission angle Ω_e by solving the relation

$$\Omega = \Omega_e + \arcsin\left(\frac{r_e \sin\Omega_e}{r}\right) - 2\arcsin\left(\frac{r_e \sin\Omega_e}{r_m}\right) \tag{30}$$

with Ω from Eq. 29. Knowing Ω and Ω_ε we obtain the Cherenkov emission angles (θ, ϕ) from the relations

$$\begin{aligned}
\cos\theta &= \frac{(zz_p + xx_p)\sin\Omega_e}{r\sin\Omega} - \frac{z_e \sin\Omega'}{r_e \sin\Omega} \\
\sin\theta\cos\varphi &= \frac{(xz_p - zx_p)\sin\Omega_e}{r\sin\Omega} - \frac{x_e \sin\Omega'}{r_e \sin\Omega} \\
\sin\theta\sin\varphi &= \frac{y\sin\Omega_e}{r\sin\Omega}
\end{aligned} \tag{31}$$

where $\Omega'=\Omega_e-\Omega$. In Fig. 23 (a), (b) we show the generated θ distributions for tracks 2, 3 of Fig. 22 (b) and in Fig. 23 (c), (d) the pattern recognized [60] and reconstructed θ distributions. Note that the reconstructed distributions are as sharp as the generated distributions (or even sharper due to pattern recognition cuts). Their intrinsic widths σ_θ are discussed in the next section.

5.4 Momentum and Mass Determination

Assuming that the mass of a particle has been determined, its momentum is obtained from $p=m\beta\gamma$. The particle velocity β is, of course, obtained from the reconstructed angle θ i.e $\beta=\cos\theta_m/\cos\theta$ with $\cos\theta_m=1/n$. Hence, the momentum precision depends on σ_θ and the reconstruction accuracy.

Using Eq.'s 27-31, the reconstructed θ was found to agree with the generated θ to within 0.01 mrad when all errors (chromatic, emission point, pixels, impact and multiple scattering) were set to zero. Hence, the reconstruction accuracy is sufficient.

The chromatic error $\sigma_\theta(E)$ is found from Eq.'s 19-24 and Tables 1-3 of [17]. A UV detector, sensitive from 6.3 to 7.1 eV (i.e $\Delta E=0.8$ eV) with an Argon gas radiator (15 bar, 20C) has chromatic error $7.0>\sigma_\theta(E)>0.7$ mrad for $10<\theta<96$ mrad (see Fig. 24). In the visible region (2 to 2.8 eV) the range is $1.6>\sigma_\theta(E)>0.2$ mrad.

The multiple scattering error $\sigma_\theta(ms)=(k_{ms}/p)\sqrt{(L/X_0)}$ depends on particle momentum p, on track pathlength L and on radiator radiation length X_0. Fig. 24 shows $\sigma_\theta(ms)$ vs θ for: (a) a 50 m track; (b) a 5 m track. Clearly, multiple scattering dominates for $\theta<90$ mrad thus σ_θ depends on particle type and so can determine mass.

From Eq. 16, we see that the momentum error of RICH depends on θ, σ_θ and N as

$$\frac{\sigma_p}{p}=\left(\frac{\sigma_\theta}{\sqrt{N}}\right)\frac{\sin\theta\cos\theta}{\sin^2\theta_m-\sin^2\theta} \tag{32}$$

since $k_r=n\beta\sigma_\theta/\sqrt{(N_0L)}=\tan\theta\sigma_\theta/\sqrt{N}$, $\cos\theta_m=1/n$, $\beta=\cos\theta_m/\cos\theta$, $\gamma=\cos\theta/\sqrt{[\sin^2\theta_m-\sin^2\theta]}$ and $p/m=\beta\gamma=\cos\theta_m/\sqrt{[\sin^2\theta_m-\sin^2\theta]}$. Thus, a track with $\theta=90$ mrad, L=25 m and $N_0=99/cm$ has N=2000 and for $\sigma_\theta\approx10$ mrad then $\sigma_p/p=1.3\%$, an excellent result if attainable.

For multiple scattering dominance (MSD) and Eq. 25 is valid thus $p=(k_{ms}/\sigma_\theta)\sqrt{(L/X_0)}$. Then Eq. 32 can be rewritten as

$$m\frac{\sigma_p}{p}=\frac{k_{ms}}{\sqrt{N_0X_0}}\frac{\cos\theta/\cos\theta_m}{\sqrt{\sin^2\theta_m-\sin^2\theta}} \tag{33}$$

to show its mass dependance. Also, we use Eq. 25 to find the mass

$$m=\frac{k_{ms}}{\sigma_\theta}\sqrt{\frac{L}{X_0}}\sqrt{\sin^2\theta_m-\sin^2\theta} \tag{34}$$

Note that Eq. 33 is independant of L because in Eq. 32 both $\sqrt{N}$ and σ_θ are proportional to $\sqrt{L}$. Note that $m(\sigma_p/p)$ depends linearly on

γ, similar to the linear p dependance of (σ_p/p) for magnetic deflection. Here, mass is determined because multiple scattering gives p and RICH gives β. This is analogous to the first measure of pion mass in emulsions i.e multiple scattering for p and range for kinetic energy $p^2/2m$.

The counter considered here can have the resolution σ_p/p given by Eq. 33 and shown in Fig. 25 for (μ, π, K, P). Clearly, (σ_p/p) is everywhere excellent ($\leq$ 1%) only reaching 1.1% for muons at θ=90 mrad corresponding to the momenta p_μ=3.1, p_π=4.2, p_K=14.7 and p_p=28.0 GeV/c. For kaons and protons MSD doesnt hold above θ=90 mrad but these momenta are already quite high for the intended neutrino beams. For muons and pions MSD extends up to $\theta\approx$95 mrad (see Fig. 24) thus to momenta p_μ=7.6, p_π=10.1 GeV/c with the still good momentum resolution of 2.6% and 2.0%, respectively. This range of momenta would be appropriate for 10-30 GeV neutrino beams.

We considered all simulated Cherenkov images from 209 above threshold tracks (70 muons, 135 pions, 4 kaons) from a mixture of 144 CC $\nu_\mu X$ and $\nu_\tau X$ interactions in Argon gas (15 bar, 20C) for E_ν from 13 to 40 GeV/c. The images were generated with chromatic errors $\sigma_\theta(E)=\Delta E/\sqrt{12}$ and detector pixel errors $\sigma_\theta(x)$, $\sigma_\theta(y)$, $\sigma_\theta(z)$. The bandwidth was ΔE=0.8 eV at $\langle E\rangle$=7.7 eV and the pixel sizes were $\Delta x=\Delta y$=30 mm and Δz=0.1 mm. The beam was constrained to interact at the middle of the radiator (z_v=25 m) but, the transverse interaction point was random ($\pm$10 m). The use of a constant L=25 m path should not bias the momentum result since Eq. 33 is L independent. The emission point error $\sigma_\theta(z_e)$ and impact parameter error $\sigma_\theta(x_e)$ are neglected since we know their contributions are much less than chromatic. In Fig. 26 we plot σ_p/p as evaluated from Eq. 32 vs θ seperately for: (a) muons; (b) pions; (c) kaons. This separation assumes that the particle mass is known (see below). The resolutions agree very well with Eq. 33 (see Fig. 25) thus showing that MSD is valid. We stress that each track has been pattern recognized [60] and reconstructed by

methods given above and so it represents a good estimate of what can be experimentally attained. We see that for a large range of θ angles (30-95 mrad) the momentum resolution is excellent (<4%).

To determine the mass spectrum, we use the reconstructed values of σ_θ, L and θ in Eq. 34 (applicable if MSD is true). The mass spectrum of the 209 track sample is shown in Fig. 27. We see the that pions and muons are nicely resolved but some overlap may remain between pions and kaons. Protons are not shown because none were produced above the high (p_p=9.7 GeV/c) threshold.

5.5 ν_τ SIGNAL AND ν_μ BACKGROUND

A simulation of 500 CC $\nu_\mu p$---μX events gave the (p, p_t) scatter plot shown in Fig. 28. Here we only required that the muon be above threshold i.e p_μ>1 GeV/c. In Fig. 29 we show 500 CC $\nu_\tau p \rightarrow \tau X$, $\tau \rightarrow \mu X'$ events again with p_μ>1GeV/c (420/500 muons pass this cut). We see a large region of low p_t events which are not present in the direct process. If we impose a cut of p_t<0.9 GeV/c (the horizontal lines in Fig.s 28-29) then 4 direct muons survive (0.8%) compared to 284 indirect muons (56.8%). However all the direct muon survivors have p<2 GeV/c and p>0.75 GeV/c hence with these cuts, zero direct muons (0%) but 280 indirect muons survive (56%). Hence, the RICH counter can strongly discriminate ν_μ events (0/500) with still good efficiency (280/500) for ν_τ events.

5.6 Counting Rates

The rates are based on a recent simulation of long baseline neutrino beams for Gran Sasso and NESTOR [62] using a 160 GeV/c proton beam on Be rod targets target followed by a 20 GeV/c coaxial horn collector. It predicts for Gran Sasso, a Gaussian ν_μ beam with rms radial width σ_r=5 km and an average neutrino energy $\langle E_\nu \rangle$=15 GeV with width $\sigma_{E\nu}$=5 GeV. The ν_e, ν_μ, ν_e contamination of this beam was 0.9%, 3.5%, 0.3%, respectively, however, this contamination is not a background for our detector. The real background is difficult to estimate but we tentatively

assume that the intrinsic ν_τ contamination of the predominantly (ν_μ, ν_e) neutrino beam is $<10^{-7}$, from tau production on the Be target with decay into the neutrino beam channel (also B production with semileptonic decay).

The number of neutrino interactions $N=AFP_{int}$ where A is the detector surface area, F the neutrino flux and $P_{int}=n\sigma L$ the ν_μ neutrino interaction probability in a target of length L, nucleon density n and neutrino cross section σ. The flux at Gran Sasso (D=731 km distant from CERN) is $F=1.1\cdot10^4$ ν/m^2 for 10^{13}-160 GeV protons on target [62]. The D dependance may be explicitly extracted i.e. $F=F_0/D^2$ where the specific flux $F_0=5.9\cdot10^9$ ν-km^2/m^2. Here, the Ar gas radiator area A=314 m^2, $n=1.5\cdot10^{22}/cm^3$, L=50 m and for $E_\nu\approx15$ GeV, $\sigma=10^{-37}$ cm^2 thus, $P_{int}\approx7.5\cdot10^{-12}$. For $3\cdot10^{19}$ protons on target per year, the specific neutrino intensity $I_0=AF_0=5.5\cdot10^{18}\nu$-km^2/y and event rate $N_0\approx42$ M events-km^2/y. Thus, at Gran Sasso only 80 ν_μ events would be produced per year.

However, with mixing, the rate equation at distance D is

$$N = N_0 M\left[\frac{\sin\left(k\Delta m^2 D / E_\nu\right)}{D}\right]^2 \tag{35}$$

where $M=\sin^2(2\alpha)$ is the energy independant mixing probability, $\Delta m^2=m_{\nu\tau}^2-m_{\nu\mu}^2$ and $k=1/4\hbar c=1.27$ GeV/km-eV^2. Note that, for small values of $k\Delta m^2D/E_\nu$, the ν_τ rate is independant of D i.e

$$N\approx N_0M(k\Delta m^2/E_\nu)^2 \tag{36}$$

This holds as long as the neutrino beam is bigger than the detector radius (10 m) i.e for D>1 km since at D=1 km, $\sigma_r=7$ m. For $E_\nu=12.7$ GeV, $\Delta m^2=10^{-2}$ eV^2 and M=1 we expect N=42 ν_τ events/y but, with 56% tagging efficiency and 18% branching ratio ($\tau\rightarrow\mu$) only $N_{obs}\approx4$ events will be observed thus probing M down to 0.5. However, for $\Delta m^2=10^{-1}$ eV^2, $N_{obs}\approx400$ and M would be probed down to 0.05.

Decreasing E_ν will increase the event rate only as E_ν^{-1} because σ is linear in E_ν moreover, this type of detector is viable only if $E_\nu>6$ GeV so that not more than a factor 2 can be gained in this way.

Since the number of oscillated events N is independant of D, it may be better strategy to place the detector at some distance D where the ν_μ rate is high and unexpected phenomena might be observed. The detector at D=2 km would see about 10^7 ν_μ events/y, about right if the ν_τ contamination level is $\approx 10^{-7}$, however, the ν_μ events would have to be efficiently identified down to the level ($1/10^7$).

Hence, a RICH radiator with 400 tons of target mass, sited anywhere between CERN and Gran Sasso ($2<D<731$) km, would probe Δm^2 down to $\approx 10^{-2}$ eV^2. Of course, if an oscillation effect is ever seen, it will suffice to change the beam energy E_ν so that both Δm^2 and $\sin^2(2\alpha)$ are measured and not just a region excluded.

It is unlikely that the $\tau \rightarrow e\nu_e\nu_\tau$ mode (18% branching ratio) can be used because the direction but not the momentum of electrons can be measured in RICH (since $\beta=1$). An electron would be characterized by $\theta \approx \theta_{max}$ and large σ_θ moreover, it could begin to shower in the Argon gas (X_0=7.85 m).

A high-energy gamma would be characterized by a conversion vertex seperate from neutrino interaction vertex and by an image with double hit density (due to the e^+e^-).

5.7 The Radiator and Detector

A deep underground tunnel could be pressurized to 15 bar to contain the Argon gas target. Surface detectors would be more difficult but large concrete bunkers (20 m diameter, 50 m length) to contain the (15 bar, 293 K) Argon gas are constructable.

The requisite mirrors with 100 m radius of curvature can be produced in 1 m^2 sections (314 are needed) and aluminized with MgF_2 overcoating for good UV reflectivity.

The large surface area tracker can be made of resistive plate chambers (RPCs) because of their good spatial resolution (σ_x=0.25

mm) and fast response (σ_t=2 ns). A large R&D effort on RPCs is being pursued for LHC and their results can be applied here.

An 80 cm thick iron filter ranges-out muons p<1 GeV/c. Its 4.7 interaction lengths leaves about 1% hadron contamination but particle ID from RICH will reduce the total to a suitably low level.

The transparency of Ar gas (ρ=.025 g/cm^3) in the (6.3 to 7.1) eV region should be good but measurements over L=50 m distance are not available. However, we have measured the transparency of liquid Krypton (ρ=2.6 g/cm^3) and found l_{abs}=3 m at E=6.7 eV [63] hence an absorption cross section σ_{Kr}=0.18 b. Since the molar refractivity of Ar is 13.3 and Kr is 21.4 at E=6.7 eV [17], we conclude that σ_{Ar}=.11 b thus l_{abs}=242 m (for ρ=.025 g/cm^3 Argon gas). This means that 77% of the photons get to the detector (for <L>=62.5 m), quite enough that the experiment remains viable.

Clearly, the most difficult part of the detector is the $3 \cdot 10^5$ photosensors. PMs would suffice nicely (even giving visible light response) but at a price of ≈300 SF (for a 25 mm ϕ PM) they would be much too expensive (90 MSF). It is not even sure that 25 mm ϕ PMs could withstand the required 15 bar pressure.

A more reasonable solution is a Fast-RICH type pad detector which can operate at 15 bars (internally and externally) with TMAE photosensor, quartz windows and gas amplification [64]. The full detector with VLSI electronics now costs ≈8 SF/ channel thus 2.4 MSF for $3 \cdot 10^5$ channels. At this level, the mechanical, tracking and optical elements would dominate total cost.

6. Conclusions

We have shown that the RICH technique is viable and responds to the essential problems of hadron (and even lepton) ID in particle physics. It suffices, for NTP gas radiators of modest length (≈2.5 m), to identify heavier particles (π, K, P) up to about 150 GeV/c. Longer radiators (≈10 m) of Helium or Neon gas can identify (π, K, P) up to about 400 GeV/c and even identify the lighter particles (e, μ, π) up to about 50 GeV/c.

We have made plausible that large RICH counters can be used to detect neutrino interactions by imaging the above threshold (γ>10) secondaries. The images determine particle momentum, direction (i.e. p and p_t), mass and charge magnitude (but not sign). Selection of $\tau \rightarrow \mu$ decays can be made by cuts in the (p, p_t) plane.

Table 1. Chromatic errors for (1 bar, 40^0 C) gas radiators with TMAE photosensor and square response between $6.1 \leq E \leq 7.1$ eV, $N_0=65/cm$ for N=9 pe's. A pixel of size Δx contributes an error $\sigma_\theta(x)=1.5\sigma_\theta(E)$.

		(μrad)	(10^{-3})	(m)	(mm)	(10^{-6})	(GeV/c)
Gas	γ_t	$\sigma_\theta(E)$	$\sigma_\theta(E)/\theta$	L	Δx	k_r	$p_{\pi K}(3\sigma)$
He	124	25	3.16	21.3	2.8	0.068	737
Ne	90	37	3.34	11.2	2.2	0.14	523
Ar	42	214	8.87	2.4	2.7	1.70	148
Kr	33	387	12.73	1.5	3.0	3.92	98
Xe	24	1331	31.40	0.8	5.5	18.48	45
N_2	41	216	8.74	2.3	2.6	1.75	145
CF_4	32	85	2.74	1.4	0.6	0.88	205
C_2F_6	25	163	4.12	0.87	0.7	2.16	131
C_5F_{12}	17	235	4.02	0.40	0.5	4.60	90

References

[1] L. Mallet, Compte Rendu 183 (1926) 274, 187 (1928) 222, 188 (1929) 445.

[2] P. A. Cherenkov, Doklady AN SSSR 3 (1936) 413, 14 (1937) 103, 14 (1937) 99, 20 (1938) 653, 21 (1938) 117, 21 (1938) 323 and Trudy Fizicheskogo Instituta AN SSSR 2 (1944) 4. See also Phys. Rev. 52 (1937) 378 for an English language publication of his early work.

[3] I .E. Tamm and I. M. Frank, Doklady AN SSSR 14 (1937) 107.

[4] V .L. Ginzburg, Zh. Eksperim. i Teor. Fiz. 10 (1940) 589 and 608.

[5] G .B. Collins and V .G. Reiling, Phys. Rev. 54 (1938) 499.

[6] H.O. Wyckoff and J. E. Henderson, Phys. Rev. 64 (1943) 1.

[7] D. Bartlett et al., Nucl. Instr. and Meth. A260 (1987) 55.

[8] A. Roberts, Nucl. Instr. and Meth. 9 (1960) 55.

[9] S. K. Poultney et al., Rev. Sci. Instr. 33 (1962) 574 and Nucl. Instr. and Meth. 20 (1963) 267.

[10] D. M. Binnie et al., Nucl. Instr. and Meth. 21 (1963) 267.

[11] P. Iredale et al., IEEE. Trans. NS11 (1964) 139.

[12] R. Giese et al., Nucl. Instr. and Meth. 88 (1970) 83.

[13] J. Seguinot, T. Ypsilantis, Nucl. Instr. and Meth. 142 (1977) 377.

[14] N. Fujiwara et al., Nucl. Instr. and Meth. A263 (1988) 381.

[15] A. P. McManus et al., Proc. Symp. on Particle ID at High Lum. Hadron Colliders, FNAL, 4/89, p597. Also M. S. Alam et al., p629.

[16] T.Ypsilantis, Physica Scripta 23 (1981) 371. See also T.Ypsilantis, CERN-EP/89-150 and Proc. Symp. on Particle ID at High Lum. Hadron Colliders. FNAL, 4/89, p133.

[17]T. Ypsilantis, J. Seguinot, Nucl. Instr. and Meth. A343 (1994) 30.

[18] J. Seguinot, T. Ypsilantis, Nucl. Instr. and Meth. A343 (1994) 1.

[19] G. Charpak and F. Sauli, Phys. Lett. 78B (1978) 523.

[20] S. Durkin, A. Honma & D.W.G.S. Leith, SLAC-PUB 2186,1978.

[21] R. Gilmore et al., Nucl. Instr. and Meth. 157 (1978) 507.

[22] G. Charpak et al., Nucl. Instr. and Meth. 164 (1979) 419.

[23] J. Seguinot, J. Tocqueville and T. Ypsilantis, Nucl. Instr. and Meth. 173 (1980) 283.

[24] T. Ekelof, J. Seguinot, J. Tocqueville and T. Ypsilantis, Physica Scripta 23 (1981) 718.
[25] D. Saloman and A. Scala, J. Chem. Phys. 62 (1975) 1469.
[26] R.A. Holroyd et al., Nucl. Instr. and Meth. A261 (1987) 440.
[27] J. Seguinot, 'Les Compteurs Cherenkov", Lectures given at l'Ecole Joliot-Curie 1988, Maubuisson, France. Published by Les Editions de Physique, 1989.
[28] G. Charpak et al., Nucl. Instr. and Meth. 180 (1981) 387.
[29] G. Coutrakon et al., IEEE Trans. Nucl. Sci. NS-29 (1982) 323. Also Nucl. Instr. and Meth. 205 (1983) 403 and 216 (1983) 79.
[30] A. Breskin et. al., IEEE Trans. Nucl. Sci. NS-35 (1988) 404.
[31] D. F Anderson, Nucl. Instr. and Meth. 178 (1980) 125. First synthesis was by H.E. Winberg, J. Am. Chem. Soc. 87 (1965) 2054.
[32] Y. Nakato et al., Bull. Chem. Soc. Jap. 45 (1971) 1299.
[33] S. Ekelin, Thesis 1981, Royal Inst. of Technology, Stockholm.
[34] E. Barrelet et. al., Nucl. Instr. and Meth. 200 (1982) 219.
[35] B. Lund-Jensen PhD thesis 1988, Univ. Uppsala, Sweden. Early reports are in Proc. Int. Conf. on High Energy Physics, Lisbon 7/81, p. 1066 & Proc. Isabelle 1981 Summer Wkshop at BNL, NY, p. 1378.
[36] R. J. Apsimon et al., IEEE. Trans. NS33 (1986) 122. Also RAL PPESP/82/24, Proposal 231, Add. 4 and M. Davenport et. al., IEEE Trans. Nucl. Sci. NS30 (1983) 35.
[37] CERN/LEPC/82-8, 31/1/82 and LEPC 82-I6 25/3/82. See also the DELPHI Technical Proposal, CERN-LEPC 83-3 and the DELPHI Progress Report, CERN-LEPC 84-16.
[38] SLD Design Reports, SLAC 273 and 274 (1984) and V. Ashford et.al., IEEE. Trans. NS33 (1986) 113.
[39] D. Dresselhaus and R. Fohrmann, Nucl. Instr. and Meth. A236 (1985) 274.
[40] J. Seguinot et al., CERN-LEPC 82/59, DELPHI 82/23 and CERN Academic Training Notes, Nov. 1982.
[41] O. Bottner et al., Nucl. Instr. and Meth. A257 (1987) 580.
[42] R. Arnold et al., Nucl. Instr. and Meth. A252 (1986) 188.
[43] R. Arnold et al., Nucl. Instr. and Meth. A270 (1988) 255.

[44] R. Arnold et al,, Nucl. Instr. and Meth. A270 (1988) 289.
[45] E. G. Anassontzis et. al., Nucl. Instr. and Meth. A323 (1992) 351.
[46] P. Baillon, Proc. 26th Int. Conf. High Energy Phys., Dallas, Texas, 8/92, p1867.
[47] K. Abe et. al., Nucl. Instr. and Meth. A343 (1994) 74.
[48] R. J. Apsimon et. al., IEEE. Trans. Nucl. Sci. NS33 (1986) 122.
[49] W. Beusch et. al., Nucl. Instr. and Meth. A323 (1992) 373.
[50] H.-W. Siebert et. al., Nucl. Instr. and Meth. A343 (1994) 60.
[51] S. Swordy, Nucl. Instr. and Meth. A343 (1994) 52.
[52] G. Coutrakon et al., IEEE Trans. Nucl. Sci. NS33 (1986) 205 and IEEE Trans. Nucl. Sci. NS35 (1988) 205.
[53] R. Baur et. al., Nucl. Instr. and Meth. A343 (1994) 99. See also P. Fischer et. al., IEEE Trans. Nucl. Sci. NS35 (1988) 432.
[54] R. Baur et. al., Nucl. Instr. and Meth. A343(1994) 231.
[55] A. Braem et. al., Nucl. Instr. and Meth. A343 (1994) 163.
[56] R. Arnold et al. Nucl. Instr. and Meth. A314 (1992). 465.
[57] J. L. Guyonnet et. al., Nucl. Instr. and Meth. A343 (1994) 178.
[58] M. French et. al., Nucl. Instr. and Meth. A324 (1993) 511 and Nucl. Instr. and Meth. A343 (1994) 222.
[59] J. Seguinot et al. Nucl. Instr. and Meth. A350 (1994) 430.
[60] D. Hatzifotiadou et. al., College de France LPC/94-29.
[61] A. Zichichi, "The Gran Sasso Project", CERN-EP/88-28.
[62] S. Katsanevas et. al, Proc. 3rd NESTOR International Conf., p504, 20/10/93, Pylos, Greece. Athens University Press.
[63] J. Seguinot, J. Tischhauser and T. Ypsilantis, "Measurements of the transmission of liquid Xenon and Krypton versus photon wavelength". In preparation.
[64] J. Seguinot, J. P. Jobez and T. Ypsilantis, "A RICH Pad Detector with TMAE gas photosensor and 2D Blinds". In preparation.

Figure Captions

Fig. 1. The ring imaging counter proposed by Roberts [8] with: **(1)** a 1-stage image intensifier; **(2)** a 2-stage gated intensifier; **(3)** a 3-stage intensifier; **(4)** a camera. Wide aperature lenses provides interstage coupling.

Fig. 2. Ring image optics for particles from an interaction region with impact parameter $x_e=0$ The detected and emitted Cherenkov angles (θ_d,θ) are equal if the detector radius is correctly chosen [13].

Fig. 3: (a) Superposition of 30 events recorded on film from the CERN hybrid MSAC; **(b)** The observed events n vs N the number of pe's/image with an <N>=1.7 normalized Poisson histogram [22]

Fig. 4: (a) The Ar gas radiator tank (L=0.94 m) with a reflective spherical mirror (f=0.94 m) and CaF_2 detector window; **(b)** The MSAC detector with gaps C-PA-T followed by a MWC=PC [24].

Fig. 5: (a) The PA gap gain vs the applied voltage (V_2-V_3); **(b)** The MWC gain vs the applied voltage $V_{pc}=V_4$; (c) The 1D ring image obtained by digital readout of the MWC wires with 2 mm pitch. The histogram is the best fit to the data [24].

Fig. 6. Quantum efficiency Q vs wavelength λ measured for: **(a)** TEA+He gas with only TEA absorbing; **(b)** TEA+CH_4 gas with both absorbing (l_{abs}=15 mm) [26, 27, 56].

Fig. 7: (a) Superposition of 300 events from the 8 m long He gas radiator and MSAC detector of the Fermilab E-605 experiment; **(b)** A single 200 GeV/c event showing the (x, y) projections of the cathode wires and the 45^0 projection of the anode wires. Matching of pulse heights allows ambiguities to be resolved for $N \leq 4$; **(c)** The π/K separation attained ($n_\sigma \approx 8.8$) at 200 GeV/c [29].

Fig. 8. The quantum efficiency Q vs wavelength λ measured for TMAE+He gas [26, 27, 33, 56].

Fig 9. Images of 500 events from 10 GeV/c pions: (left) observed and (right) simulated in the Ar gas radiator with the long drift-TPC-MWC detector. The images are sharper than shown because the beam had non-zero divergence. The snow around the images is due to photon feedback [34, 35].

Fig. 10. The first proximity-focused liquid C_6F_{14} radiator with a long drift TPC coupled to the MWCs at the end of each drift volume and filled with CH_4+i-C_4H_{10}+TMAE gas at NTP. The drift volume end metal plates prevent the beam ionization electrons to enter the drift volume [40].

Fig. 11. The original design of the DELPHI Barrel RICH showing the parabolic mirrors, the 1.6 m long drift volume, the field shaping traces, the MWCs and the two radiator media [40].

Fig. 12: (a) The geometry of the proximity-focused liquid C_6F_{14} ring image and the mirror focused gas image; **(b)** Superposed images from 100-10 GeV/c pion tracks at normal incidence showing a large liquid ring, a much smaller gas ring and the beam traces [42].

Fig. 13. The reconstructed Cherenkov angle θ in DELPHI Barrel RICH from hadrons in jets at LEP: **(a)** from the liquid C_6F_{14} radiator; **(b)** after background subtraction [45].

Fig. 14. Scatter plots of the reconstructed Cherenkov angle θ vs momentum p of hadrons in jets seen by DELPHI Barrel RICH at LEP from: **(a)** the liquid C_6F_{14} radiator; **(b)** the gas radiator [45].

Fig. 15. The geometry of the Ω-RICH counter with 31 m^2 of hexagonal mirrors and 11 m^2 of quartz windowed drift space [36].

Fig. 16. Events from the upgraded Ω-RICH between 50-55 GeV/c vs ring radius with the fit curves for p, K and π [55].

Fig. 17. Cathode pad detector options: **(a)** a MSAC with gaps C-PA-T-PA-T and electron collection on the pads; **(b)** an asymmetric MWC with wire amplification and an induced pad signal.

Fig. 18. A scatter plot of 2000 superposed images from 10 GeV/c pions at $\theta_p=25^0$ in 10 mm thick LiF as seen by the Fast-RICH pad detector and readout with digital VLSI electronics. Each sector is 900 mm long, 156 mm wide with 3840 pads of 5.3 x 6.6 mm^2. The central spot is the beam and the "smile" the ring image. The small amount of "fuzz" is due to weak scintillation of the LiF [59].

Fig. 19. Two single 10 GeV/c events from the preceeding scatter plot. Each large rectangle has 16 individual pads. Note that the events are clean with little noise or feedback [59].

Fig. 20. The reconstructed Cherenkov θ angle from events of the preceeding figures, fit with $\langle\theta\rangle$=839 mrad, σ_θ=13.9 mrad/photon and a small background due to LiF scintillation [59].

Fig. 21. A schematic view of a long baseline RICH radiator, mirror and detector along with an external tracker and muon filter.

Fig. 22. Stereographic images for events with E_ν=40 GeV, z=25 m:

(a) $\nu_\tau X \to \tau^- \rho^0 \rho^0 \eta' \pi^+ p$, $\tau^- \to \nu_\tau \rho^- \to \nu_\tau \pi^- \pi^0$, $\rho^0 \to \pi^+\pi^-$, $\eta' \to \pi^+\pi^-\eta$, $\eta \to 3\pi^0$;

(b) $\nu_\mu p \to \mu^- \rho^+ \eta' \Delta^+ \pi^0$, $\rho^+ \to \pi^+\pi^0$, $\Delta^+ \to \pi^+\pi^0$, $\eta' \to \gamma\rho^0 \to \gamma\pi^+\pi^-$.

Fig. 23. Distributions of Cherenkov angle θ for tracks 2, 3 of Fig. 22b: **(a), (b)** generated; **(c), (d)** reconstructed.

Fig. 24. The multiple scattering error σ_θ vs θ for μ, π, K, P with, for comparison, the UV chromatic error at $\langle E\rangle$=6.7 eV, ΔE=0.8 eV: **(a)** for 50 m pathlength; **(b)** for 5 m pathlength.

Fig. 25. The momentum resolution σ_p/p vs Cherenkov angle θ for μ, π, K, P assuming errors are from multiple scattering (Eq. 33).

Fig. 26. Momentum resolution σ_p/p vs θ for all tracks from 209 CC νX events with measurement and multiple scattering errors, plotted for μ, π and Ks and compared to the MSD line of Eq. 33.

Fig. 27. The mass spectrum for the tracks of the preceeding figure. The mass was calculated via Eq. 34 from σ_θ, L and reconstructed θ. The μ, π and K tracks are grey, white and black, respectively.

Fig. 28. Scatter plots of (p_t, p) for 500 CC events with E_ν=20 GeV: **(a)** $\nu_\mu p \to \mu X$ events; **(b)** $\nu_\tau p \to \tau X$, $\tau \to \mu X'$ events. The horizontal and vertical lines show selection cuts.

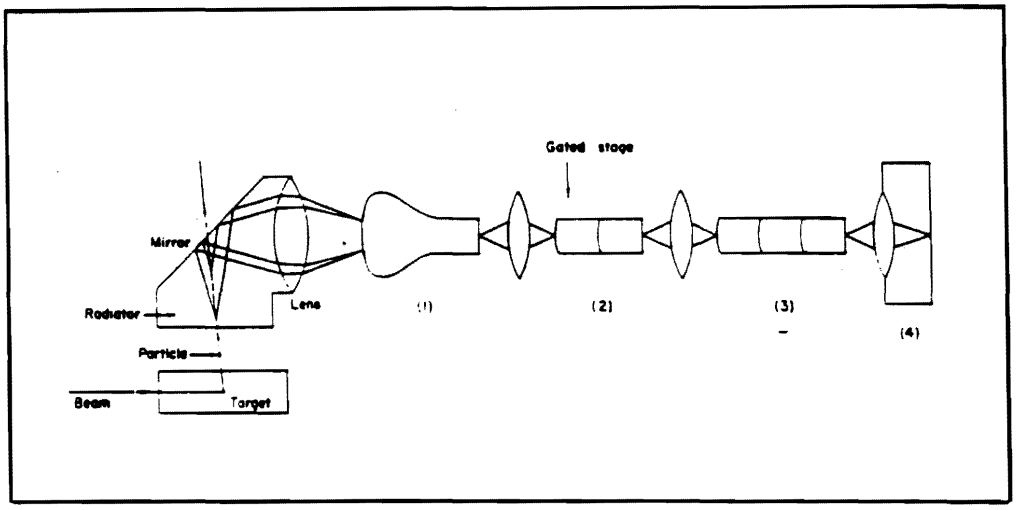

Fig. 1. The ring imaging counter proposed by Roberts [8] with: **(1)** a 1-stage image intensifier; **(2)** a 2-stage gated intensifier; **(3)** a 3-stage intensifier; **(4)** a camera. Wide aperature lenses provides interstage coupling.

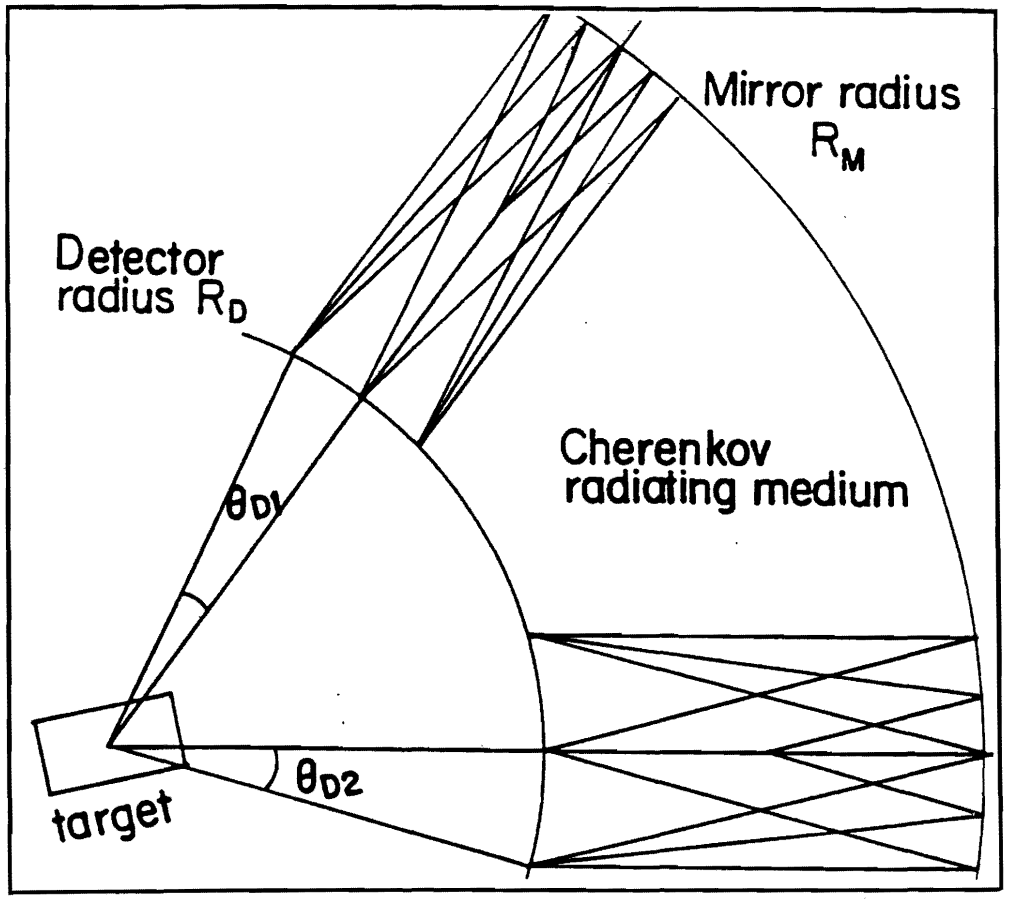

Fig. 2. Ring image optics for particles from an interaction region with impact parameter x_e=0 The detected and emitted Cherenkov angles (θ_d,θ) are equal if the detector radius is correctly chosen [13].

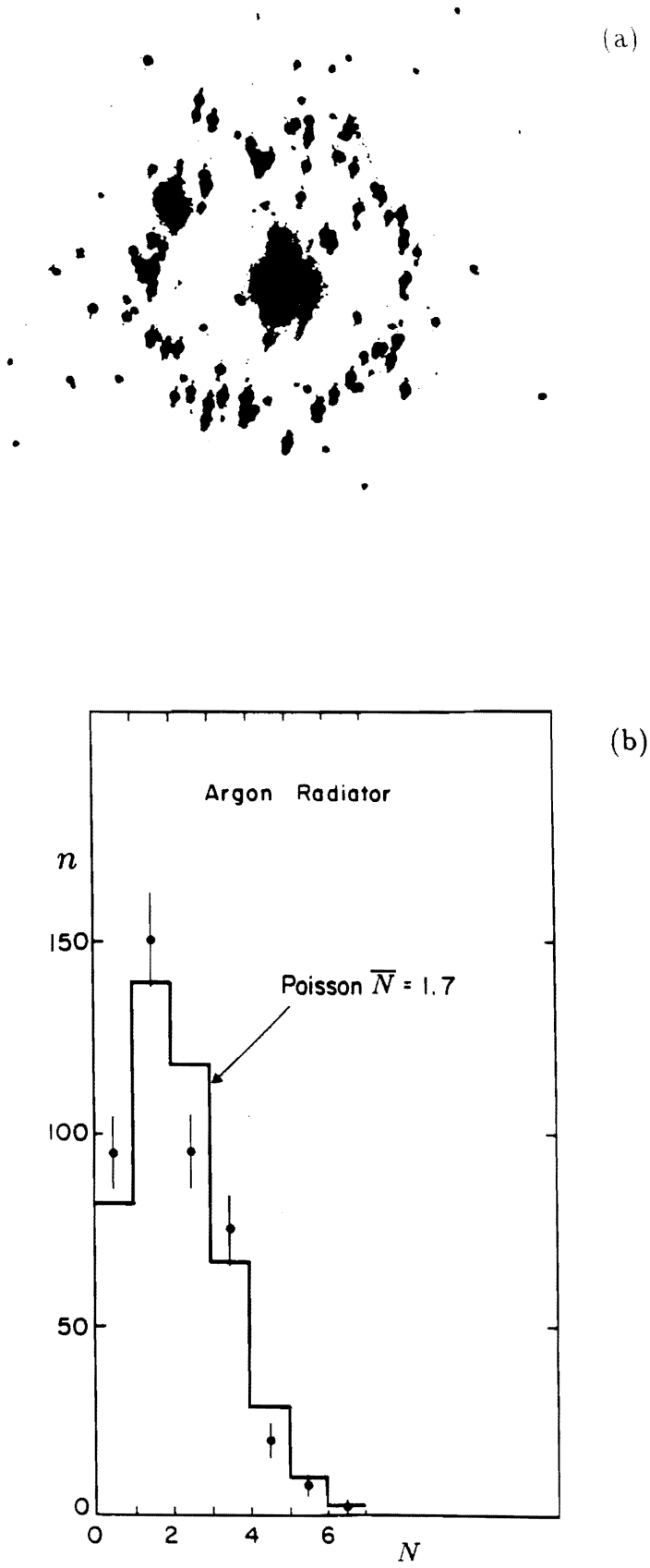

Fig. 3: (a) Superposition of 30 events recorded on film from the CERN hybrid MSAC; **(b)** The observed events n vs N the number of pe's/image with an <N>=1.7 normalized Poisson histogram [22]

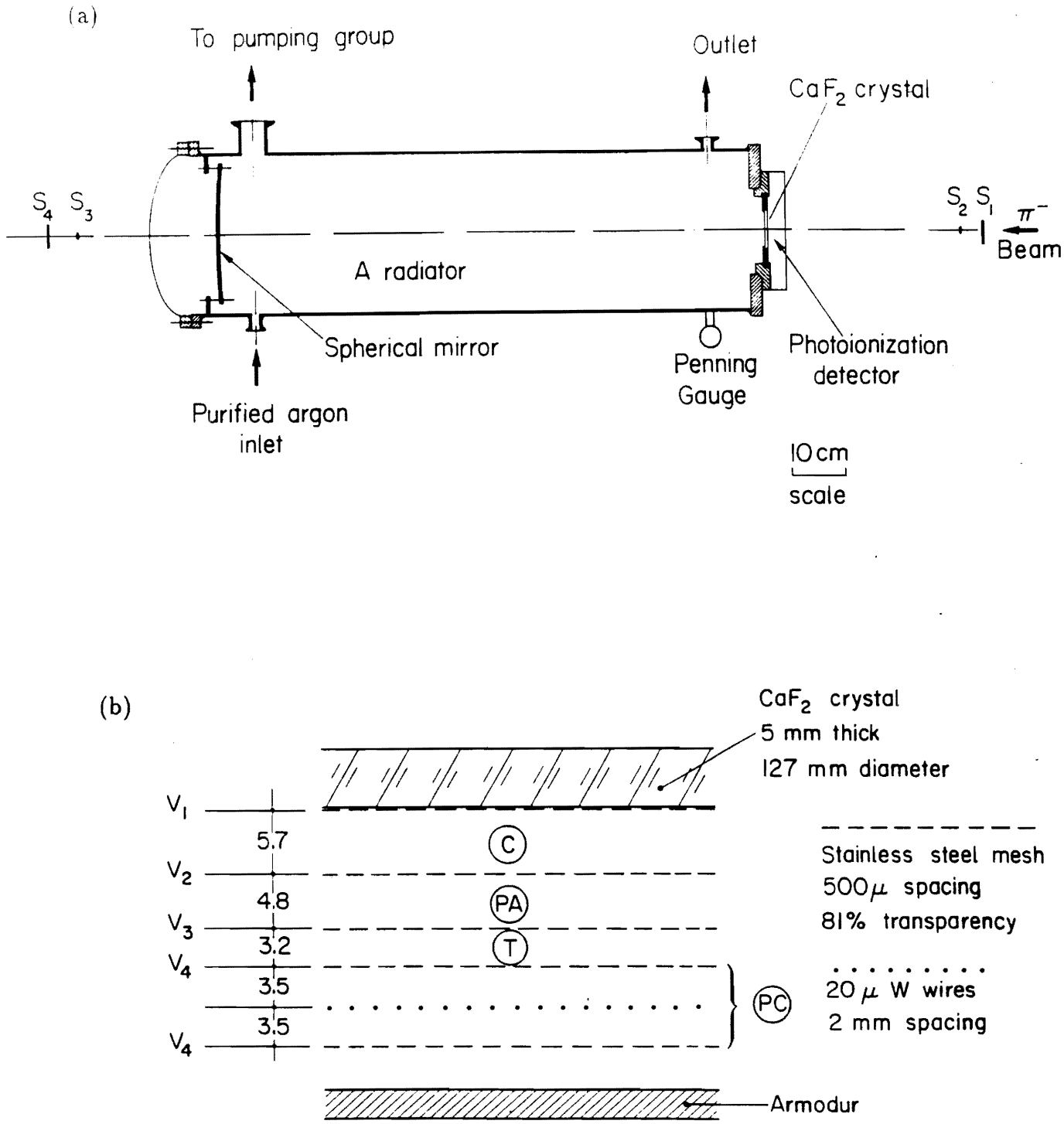

Fig. 4: (a) The Ar gas radiator tank (L=0.94 m) with a reflective spherical mirror (f=0.94 m) and CaF_2 detector window; **(b)** The MSAC detector with gaps C-PA-T followed by a MWC=PC [24].

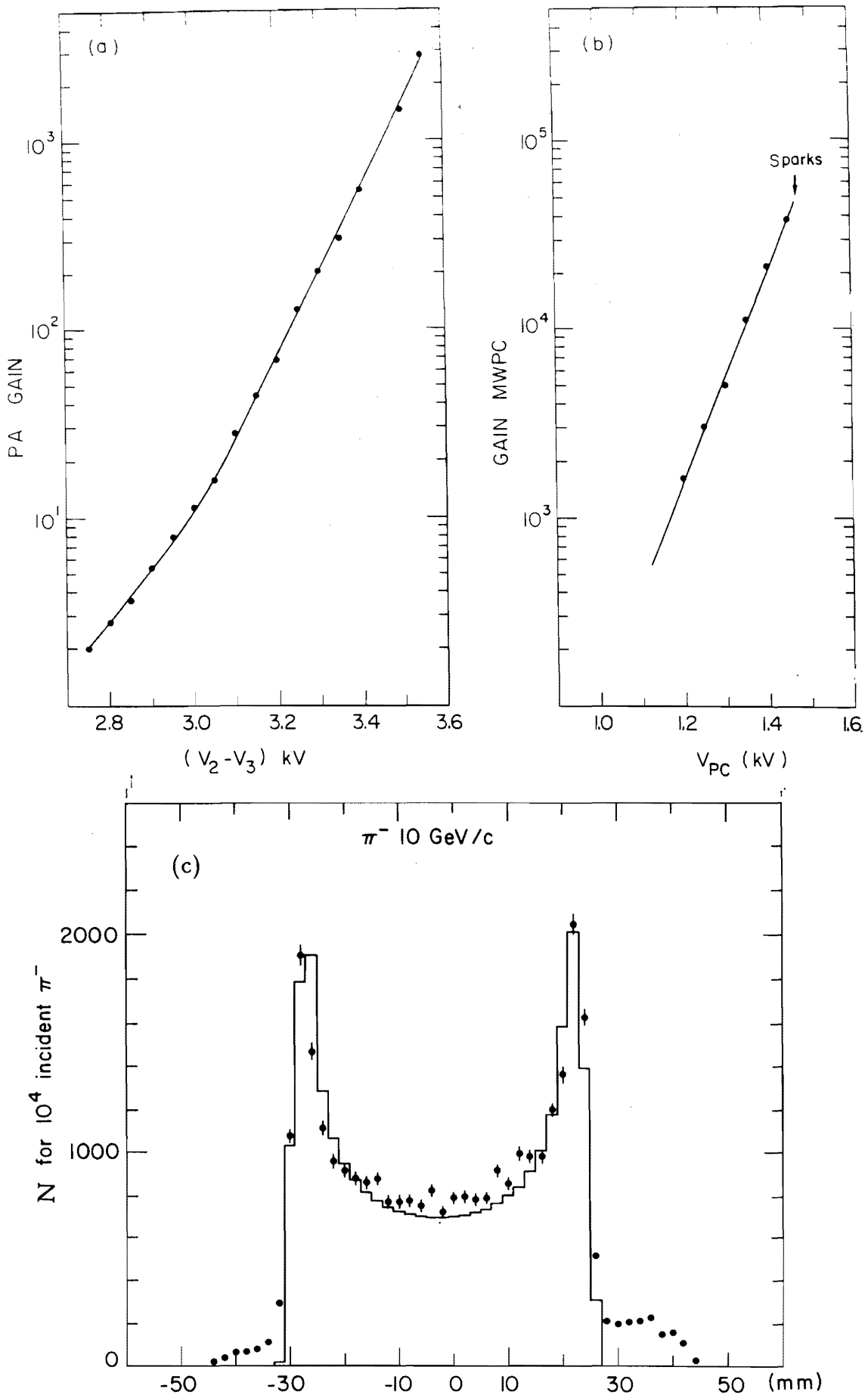

Fig. 5: (a) The PA gap gain vs the applied voltage (V_2-V_3); **(b)** The MWC gain vs the applied voltage V_{pc}=V_4; (c) The 1D ring image obtained by digital readout of the MWC wires with 2 mm pitch.

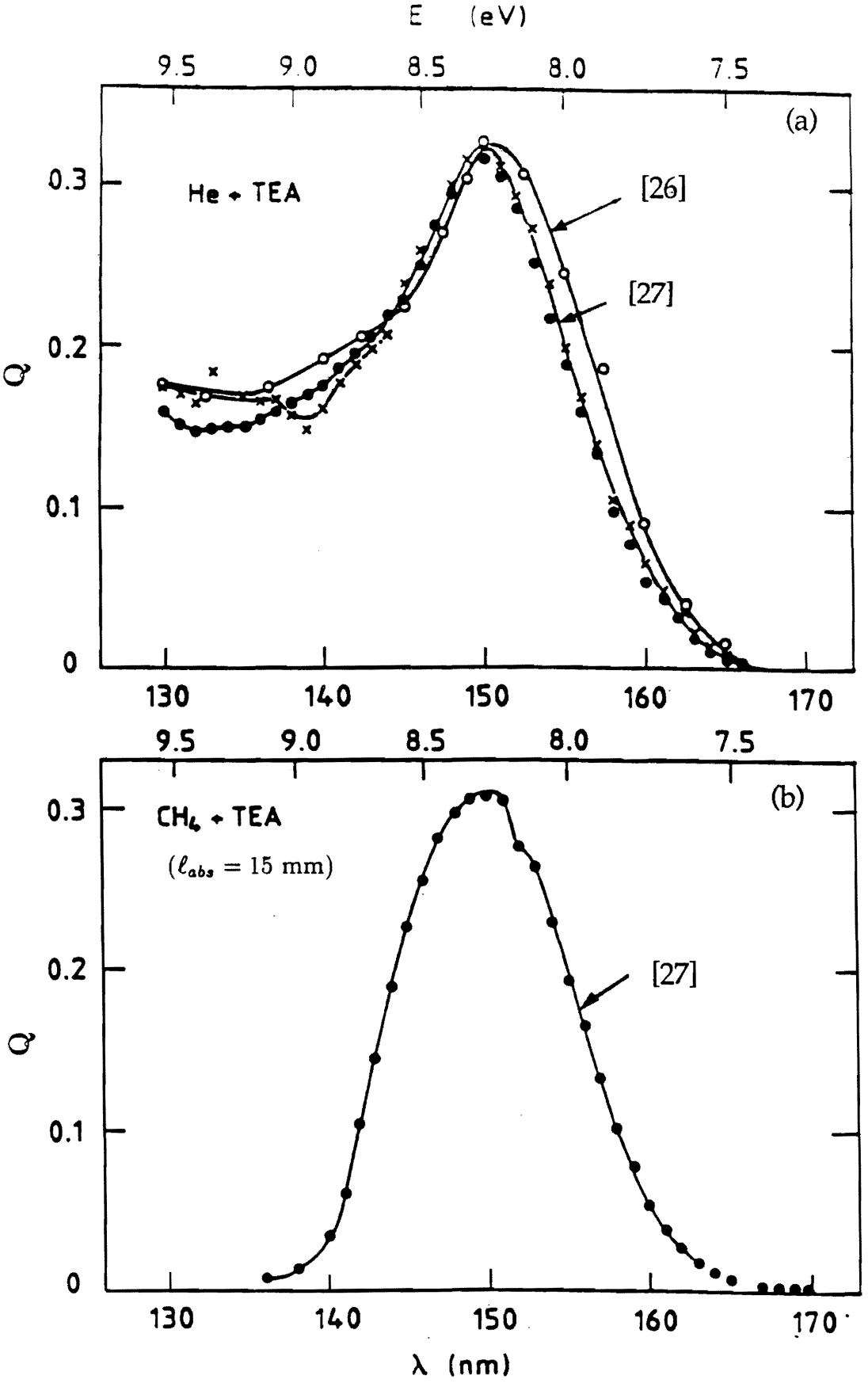

Fig. 6. Quantum efficiency Q vs wavelength λ measured for: **(a)** TEA+He gas with only TEA absorbing; **(b)** TEA+CH_4 gas with both absorbing (l_{abs}=15 mm) [26, 27, 56].

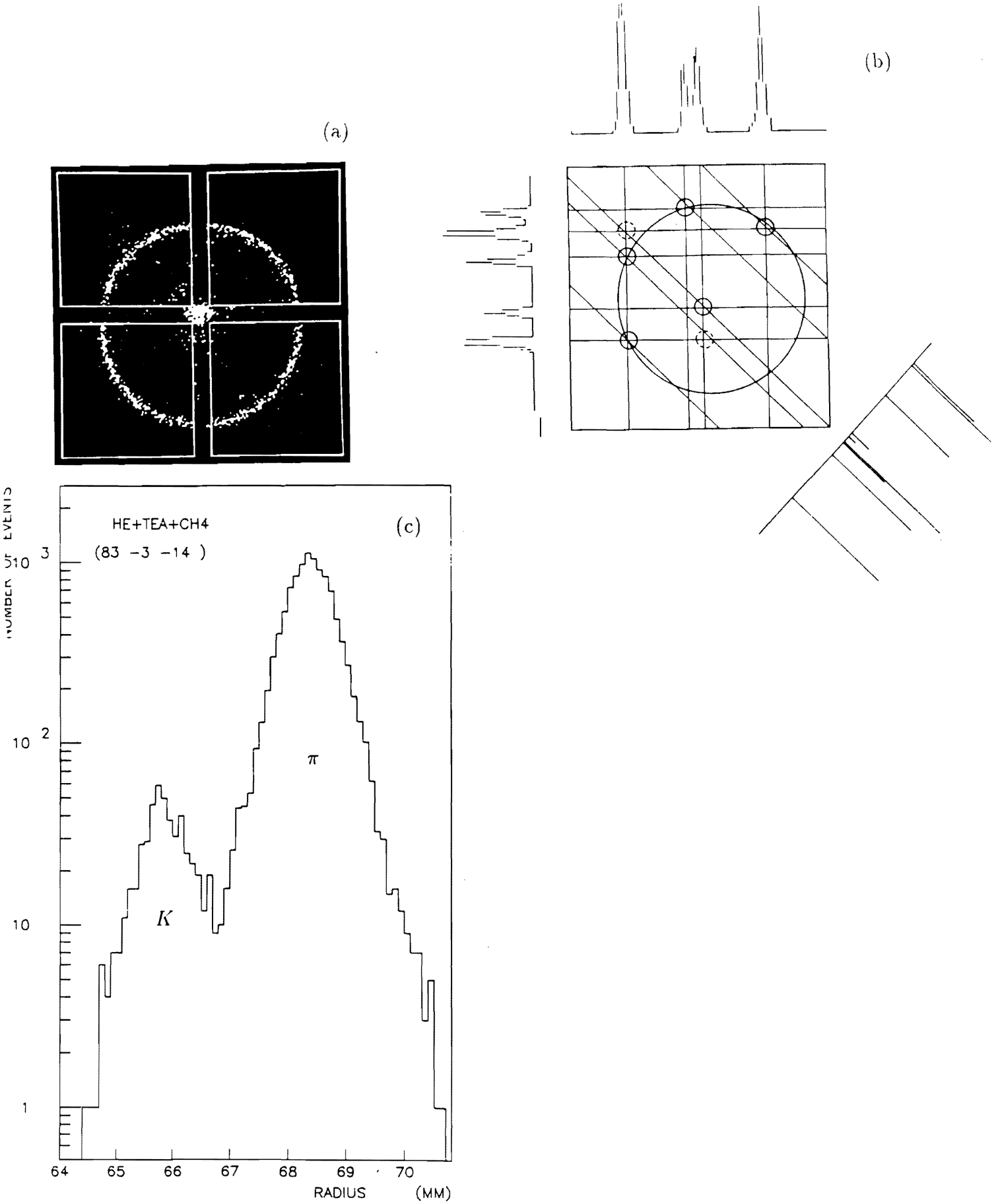

Fig. 7: **(a)** Superposition of 300 events from the 8 m long He gas radiator and MSAC detector of the Fermilab E-605 experiment; **(b)** A single 200 GeV/c event showing the (x, y) projections of the cathode wires and the 45^0 projection of the anode wires. Matching of pulse heights allows ambiguities to be resolved for $N \leq 4$; **(c)** The π/K separation attained ($n = 8.8$) at 200 GeV/c [20].

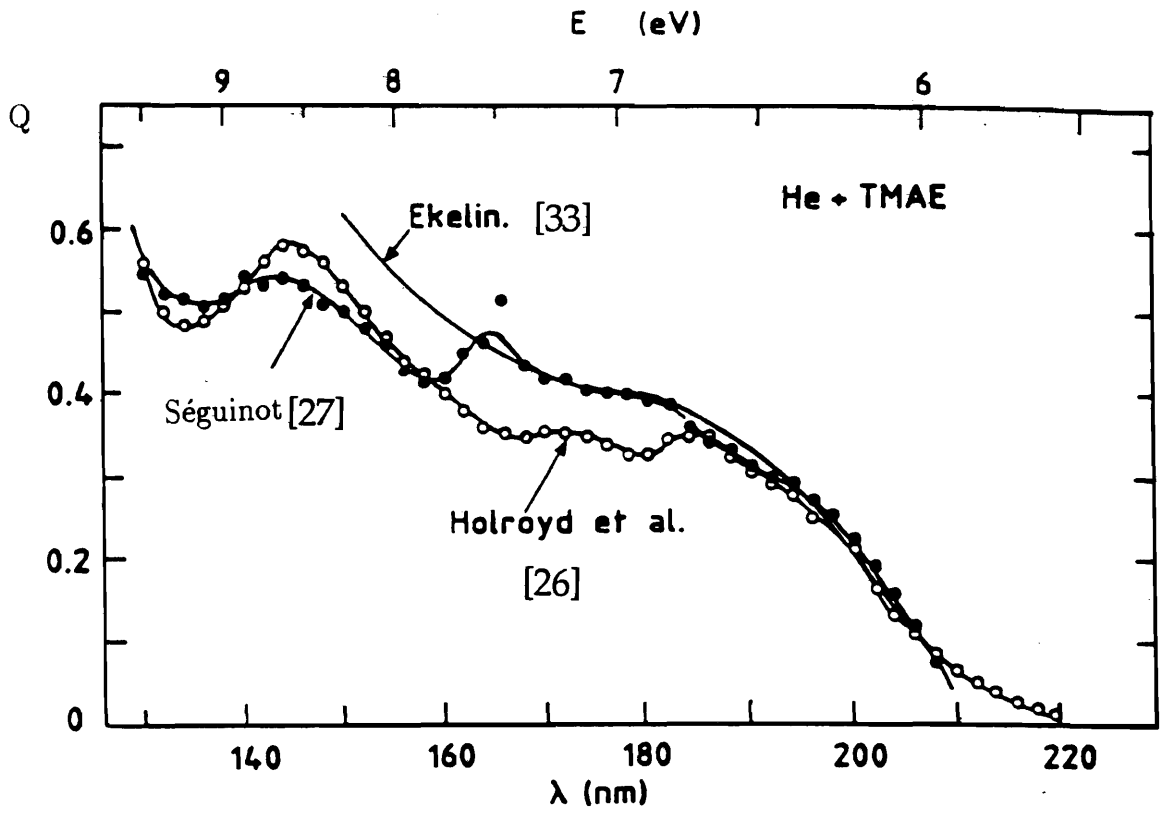

Fig. 8. The quantum efficiency Q vs wavelength λ measured for TMAE+He gas [26, 27, 33, 56].

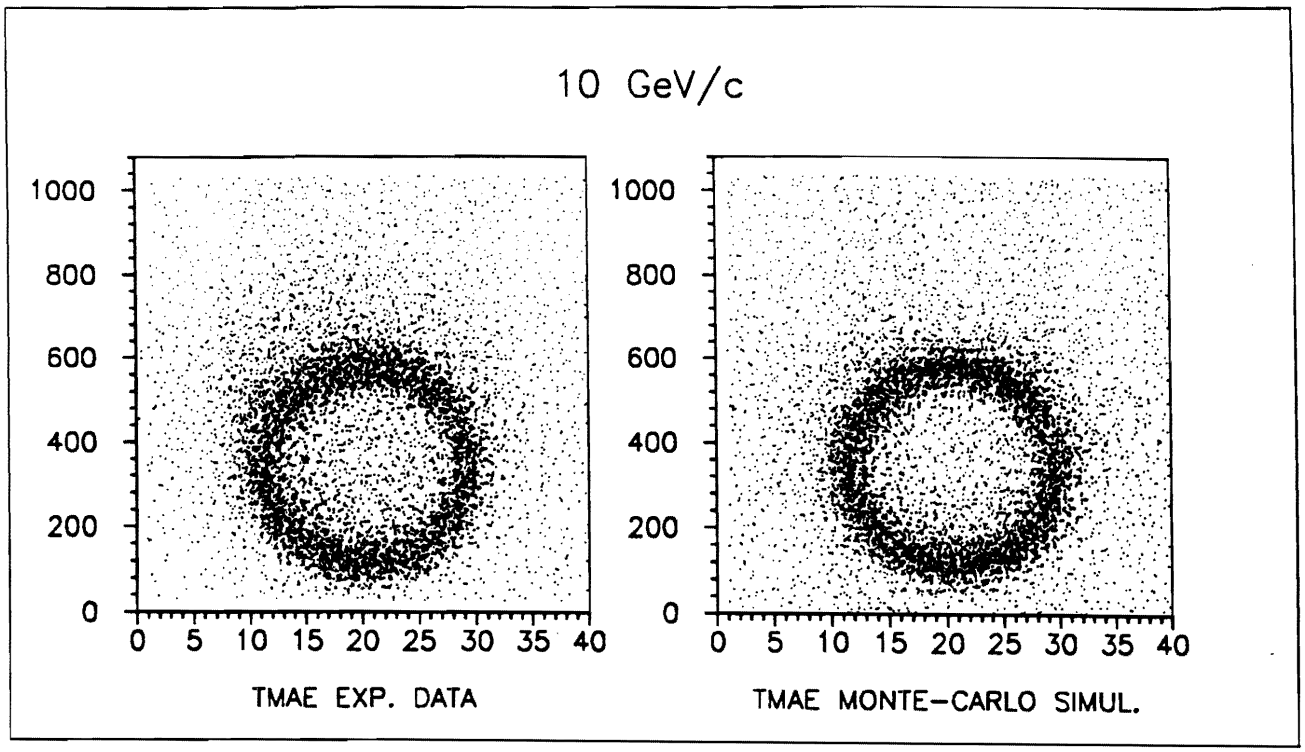

Fig 9. Images of 500 events from 10 GeV/c pions: (left) observed and (right) simulated in the Ar gas radiator with the long drift-TPC-MWC detector. The images are sharper than shown because the beam had non-zero divergence. The snow around the images is due to photon feedback [34, 35].

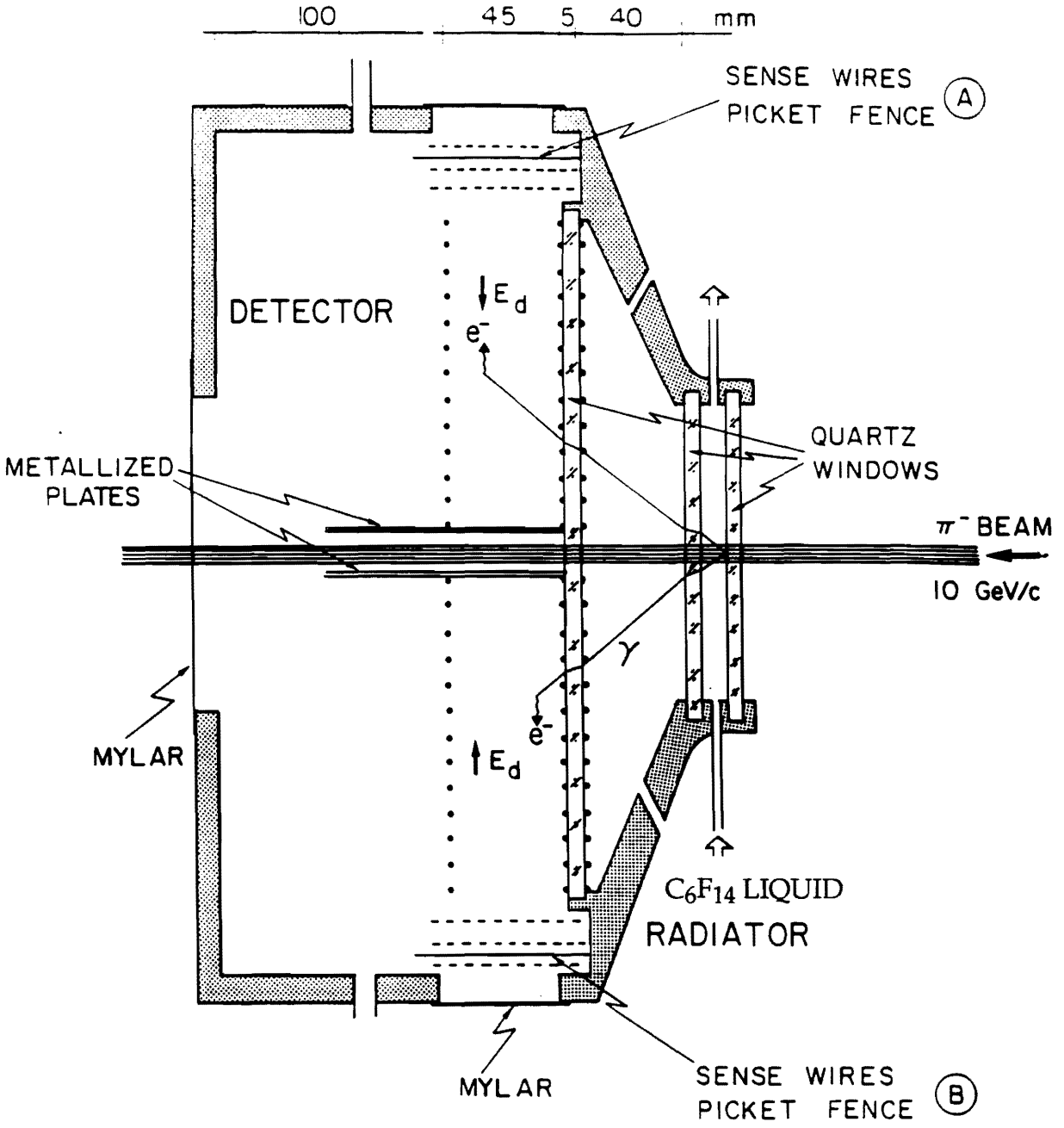

Fig. 10. The first proximity-focused liquid C_6F_{14} radiator with a long drift TPC coupled to the MWCs at the end of each drift volume and filled with CH_4+i-C_4H_{10}+TMAE gas at NTP. The drift volume end metal plates prevent the beam ionization electrons to enter the drift volume [40].

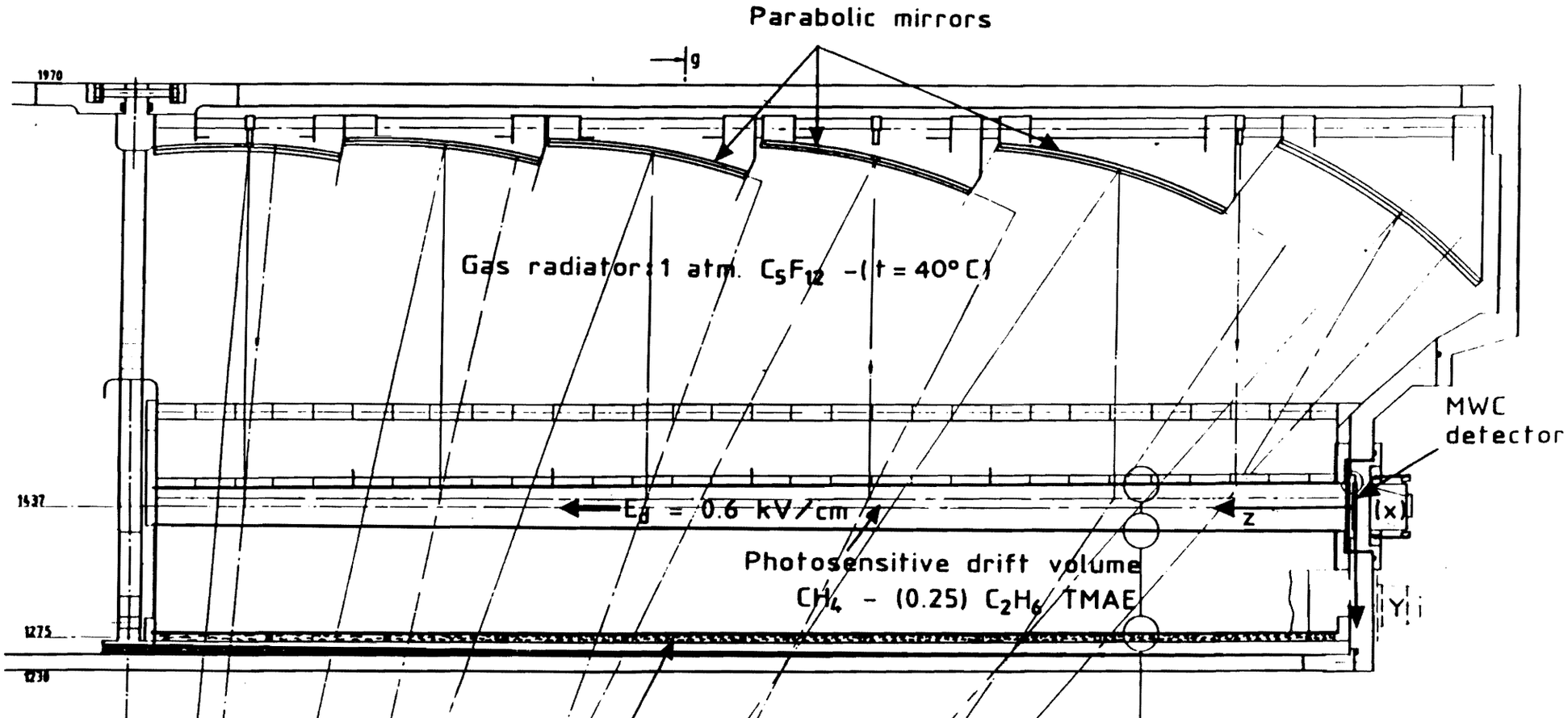
Parabolic mirrors
9
1970
Gas radiator: 1 atm. C_5F_{12} - (t = 40° C)
MWC
detector
1537
E_d = 0.6 kV/cm
z
(x)
Photosensitive drift volume
CH_4 - (0.25) C_2H_6 TMAE
Y
1275
1230

(a)

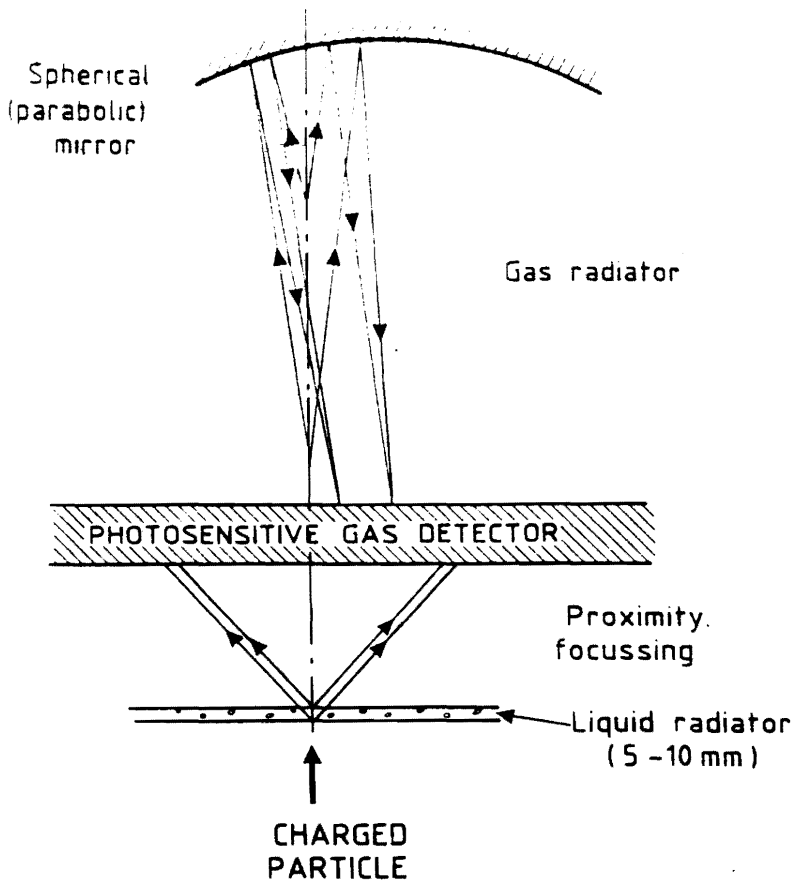

(b)

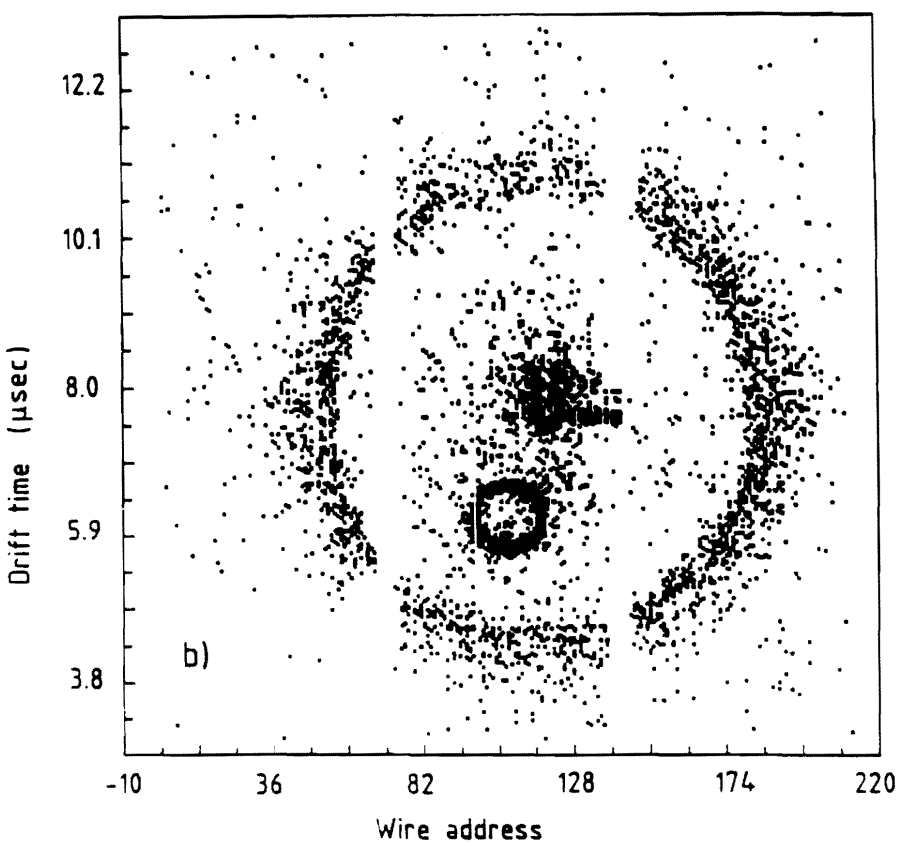

Fig. 12: (a) The geometry of the proximity-focused liquid C_6F_{14} ring image and the mirror focused gas image; **(b)** Superposed images from 100-10 GeV/c pion tracks at normal incidence showing a large liquid ring, a much smaller gas ring and the beam trace [42].

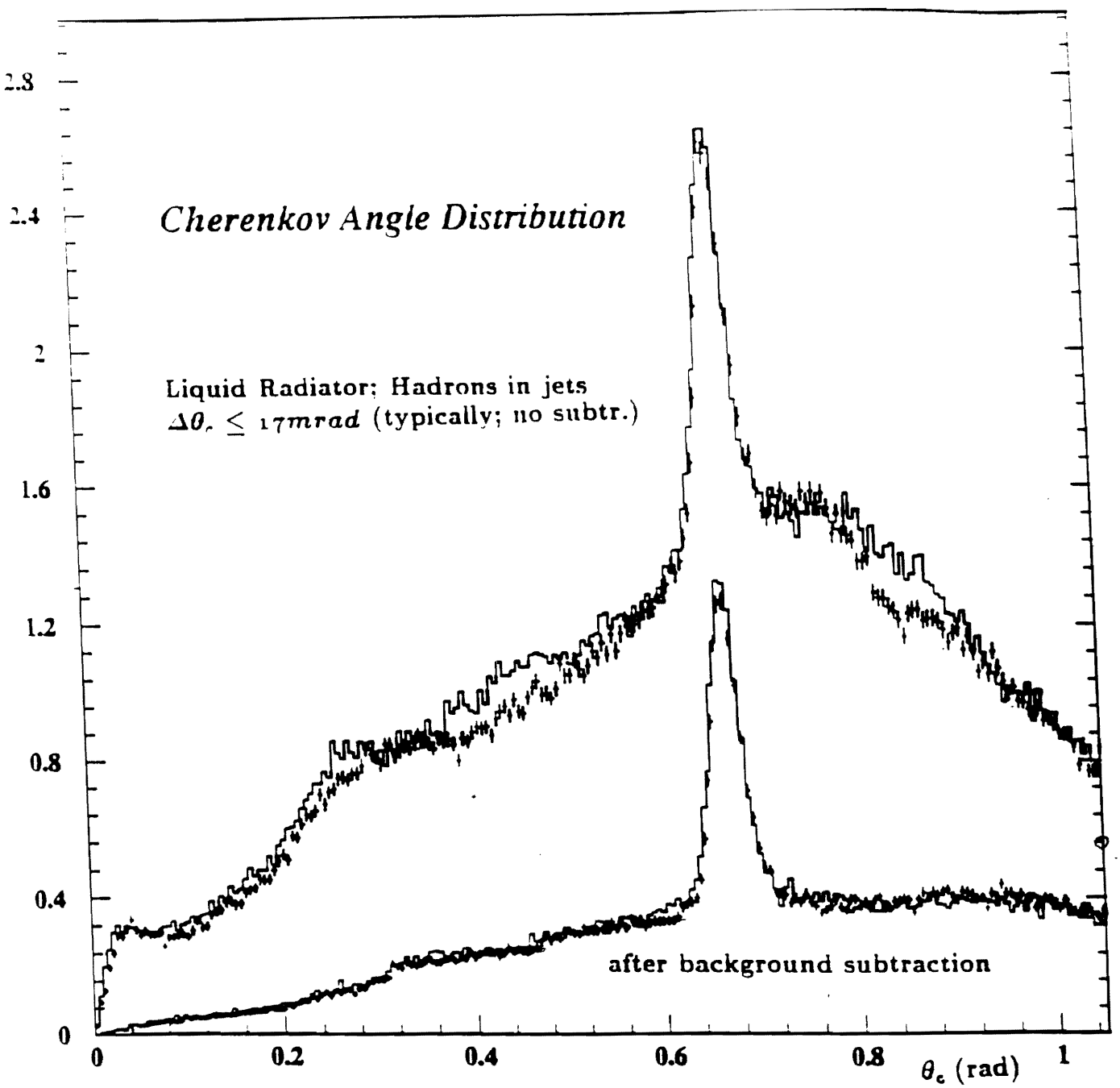

Fig. 13. The reconstructed Cherenkov angle θ in DELPHI Barrel RICH from hadrons in jets at LEP: **(a)** from the liquid C_6F_{14} radiator; **(b)** after background subtraction [45].

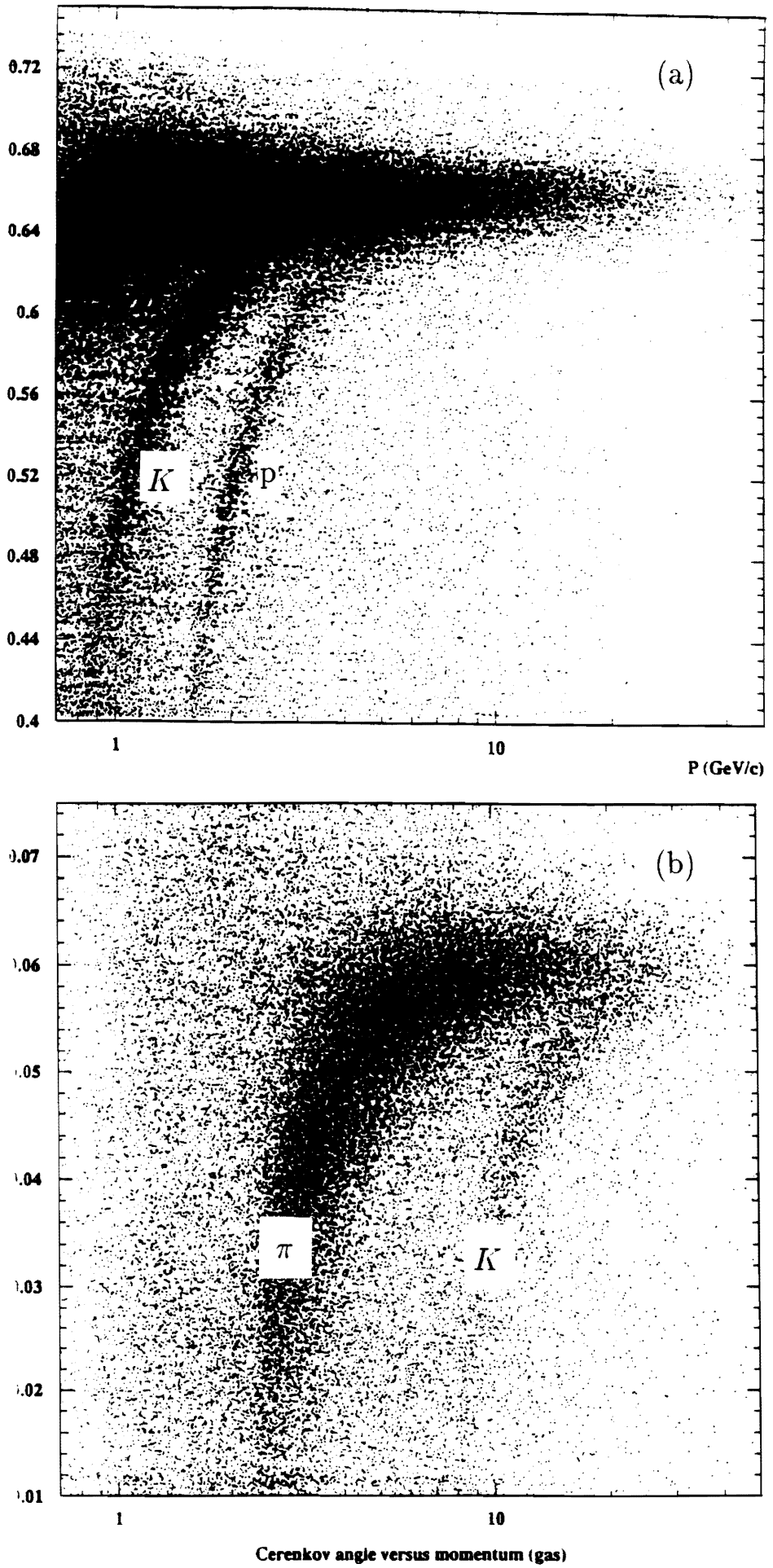

Fig. 14. Scatter plots of the reconstructed Cherenkov angle θ vs momentum p of hadrons in jets seen by DELPHI Barrel RICH at LEP from: **(a)** the liquid C_6F_{14} radiator; **(b)** the gas radiator [45].

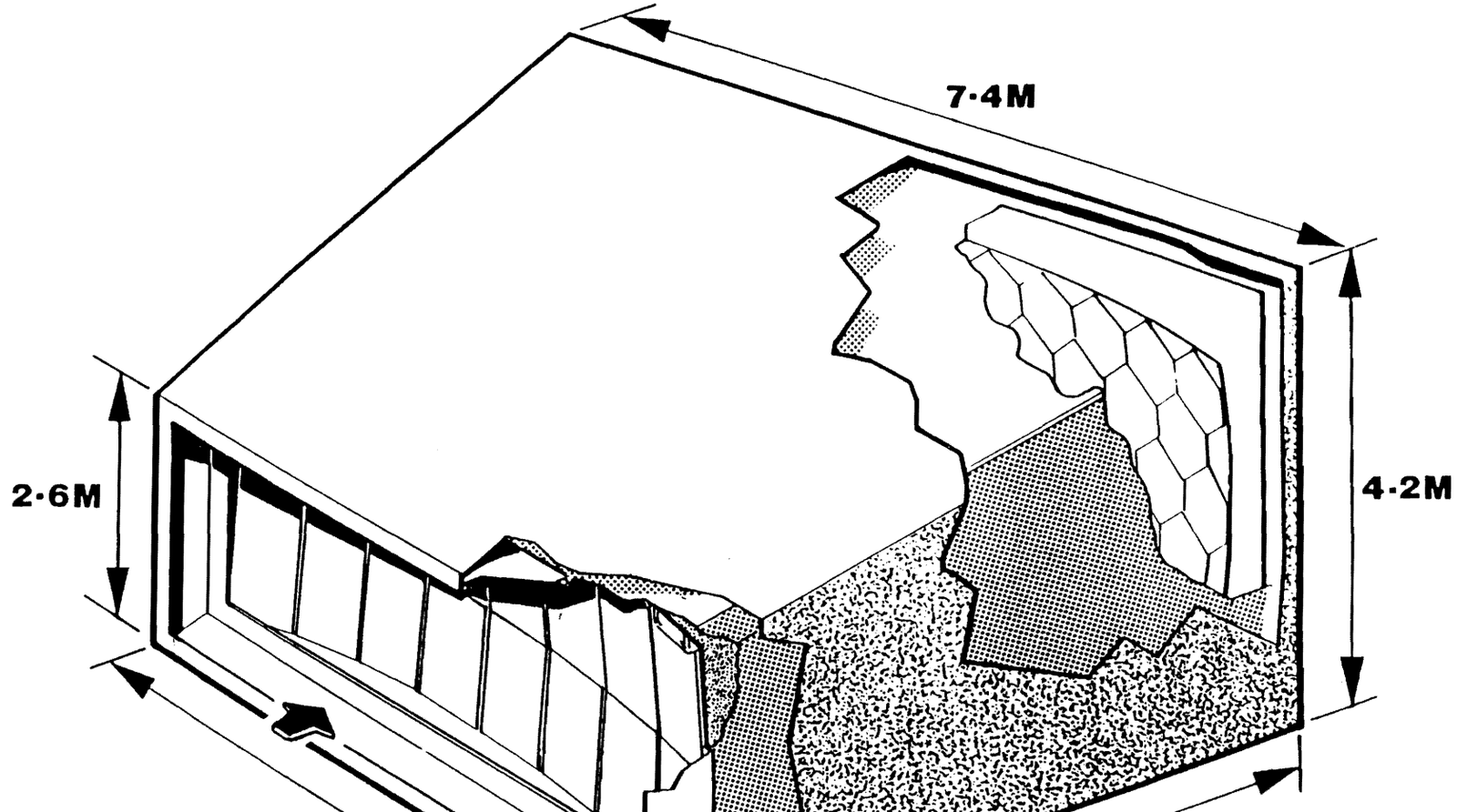
7·4M
2·6M
4·2M

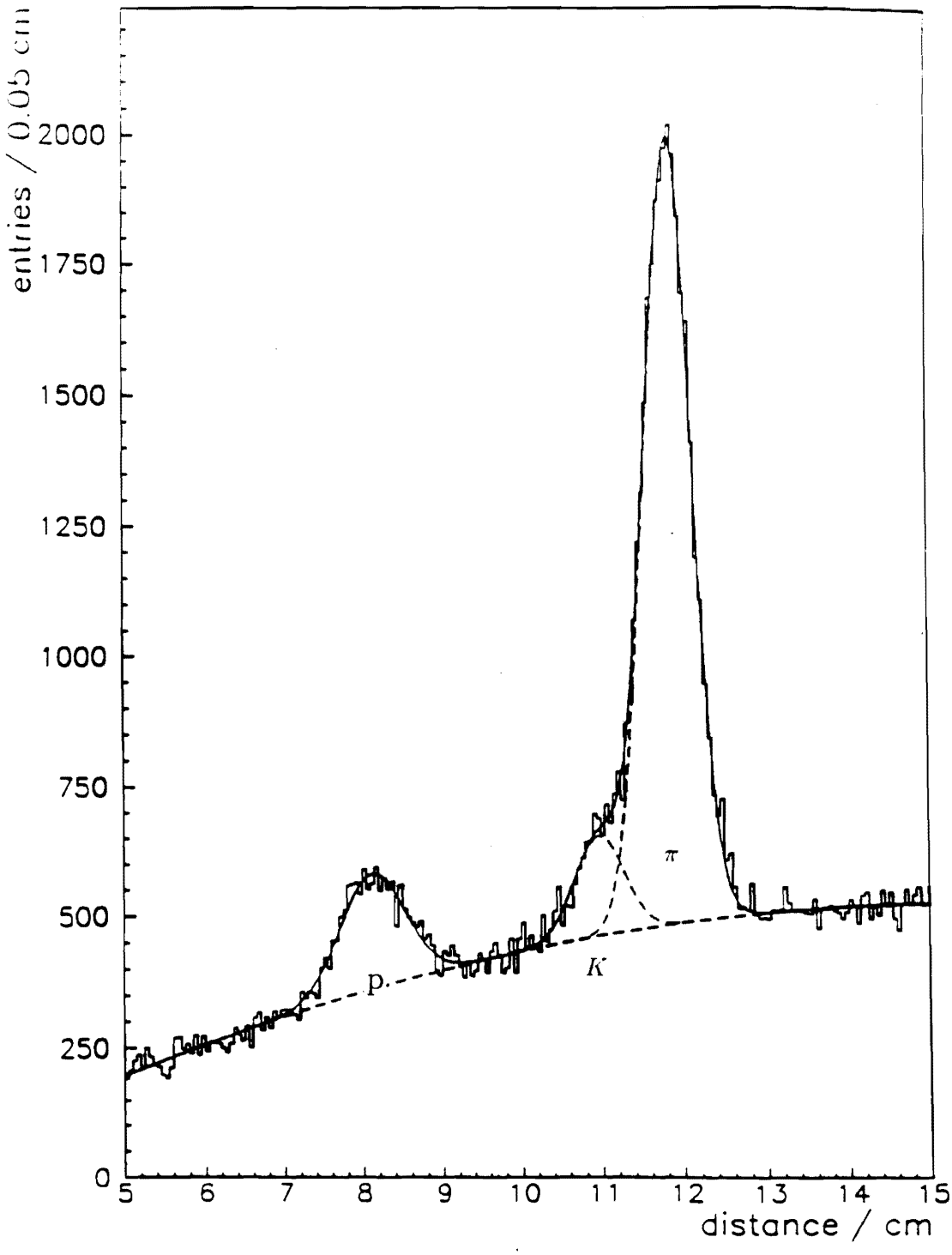

Fig. 16. Events from the upgraded Ω-RICH between 50-55 GeV/c vs ring radius with the fit curves for p, K and π [55].

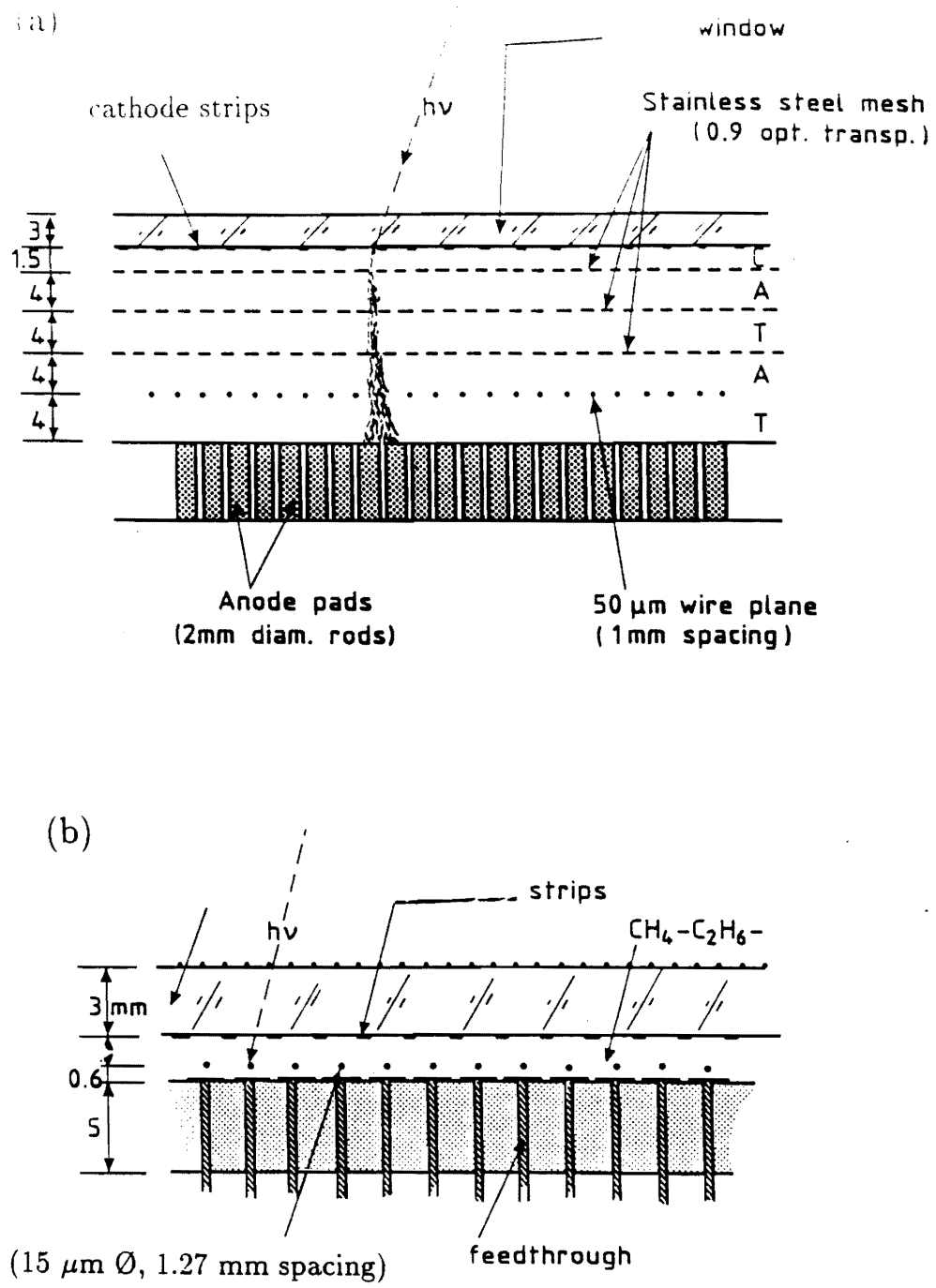

Fig. 17. Cathode pad detector options: **(a)** a MSAC with gaps C-PA-T-PA-T and electron collection on the pads; **(b)** an asymmetric MWC with wire amplification and an induced pad signal.

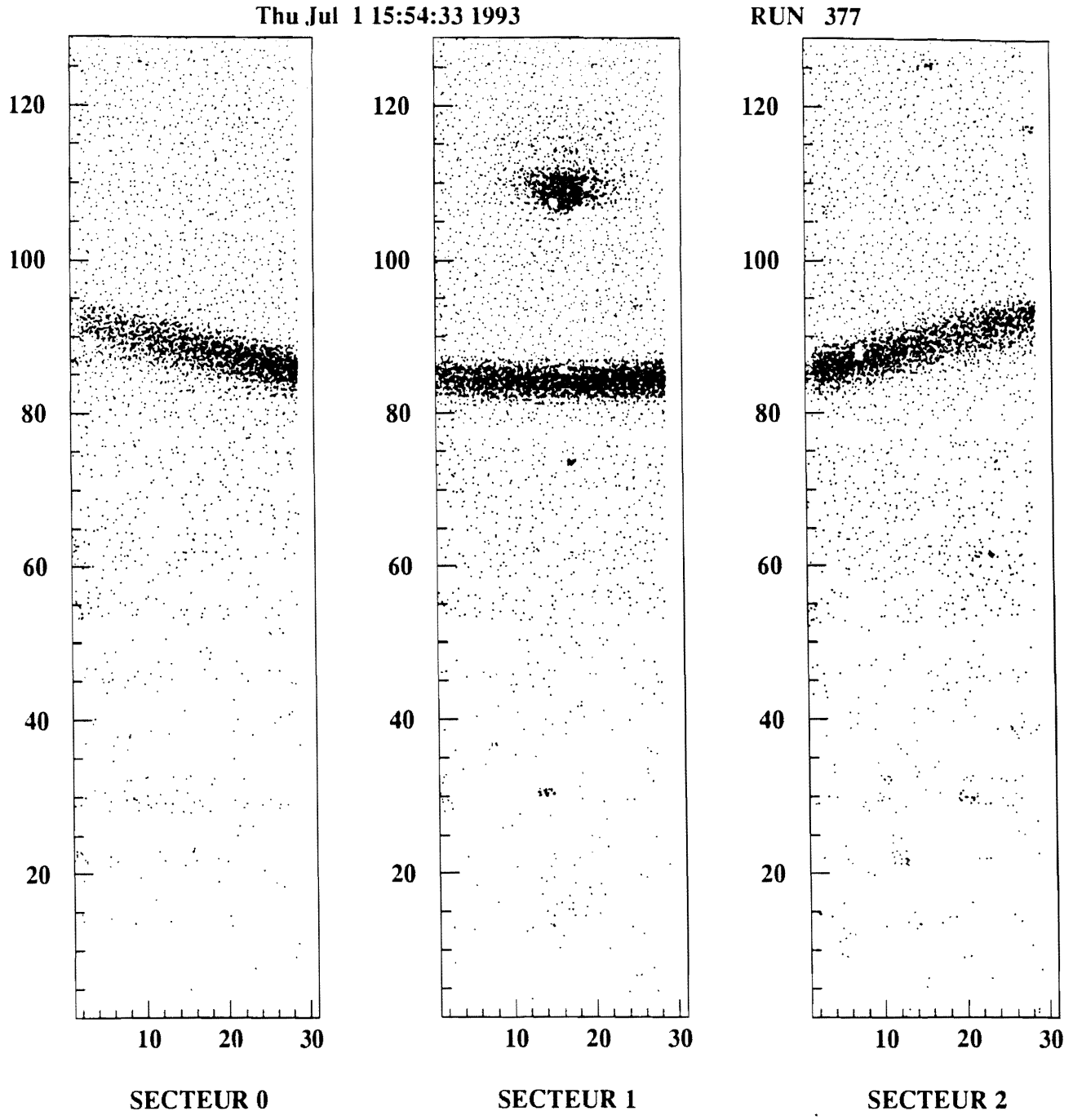

Fig. 18. A scatter plot of 2000 superposed images from 10 GeV/c pions at $\theta_p=25^0$ in 10 mm thick LiF as seen by the Fast-RICH pad detector and readout with digital VLSI electronics. Each sector is 900 mm long, 156 mm wide with 3840 pads of 5.3 x 6.6 mm^2. The central spot is the beam and the "smile" the ring image. The small amount of "fuzz" is due to weak scintillation of the LiF [59].

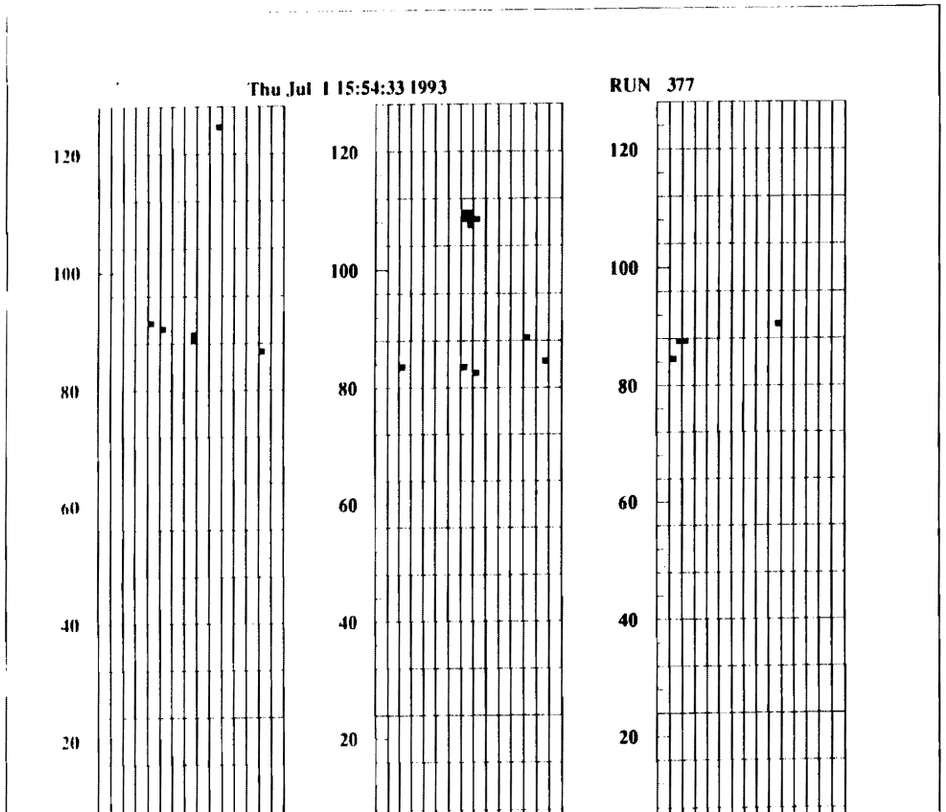
Thu Jul 1 15:54:33 1993
RUN 377
120
100
80
60
40
20

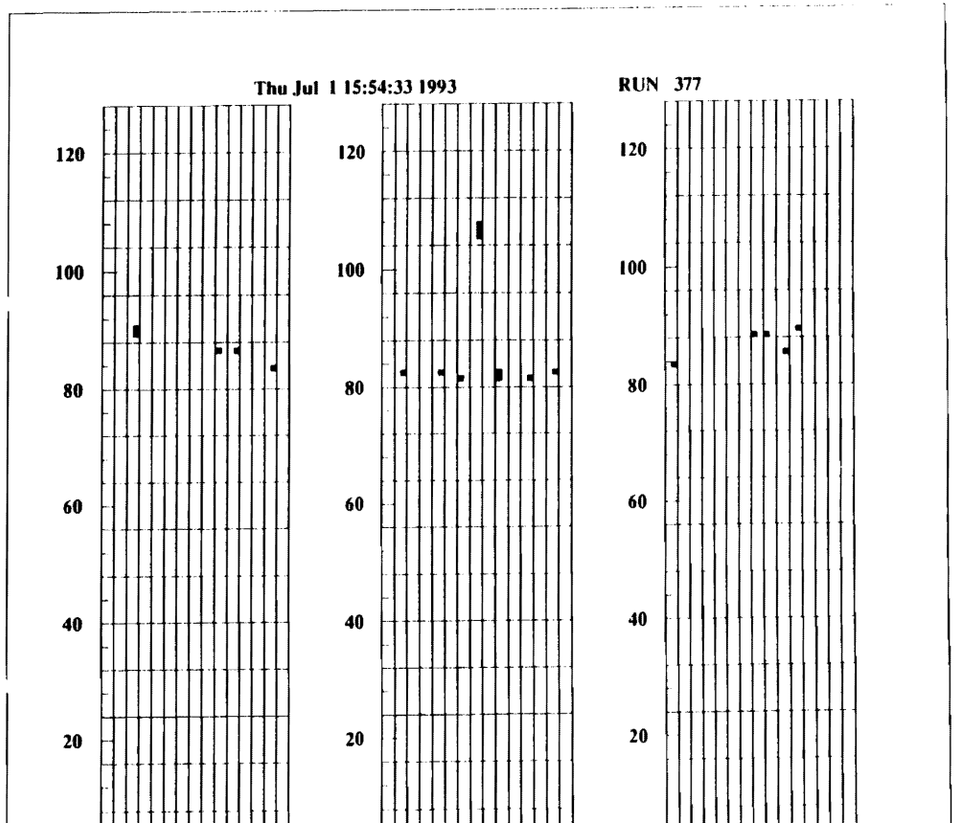
Thu Jul 1 15:54:33 1993
RUN 377
120
100
80
60
40
20

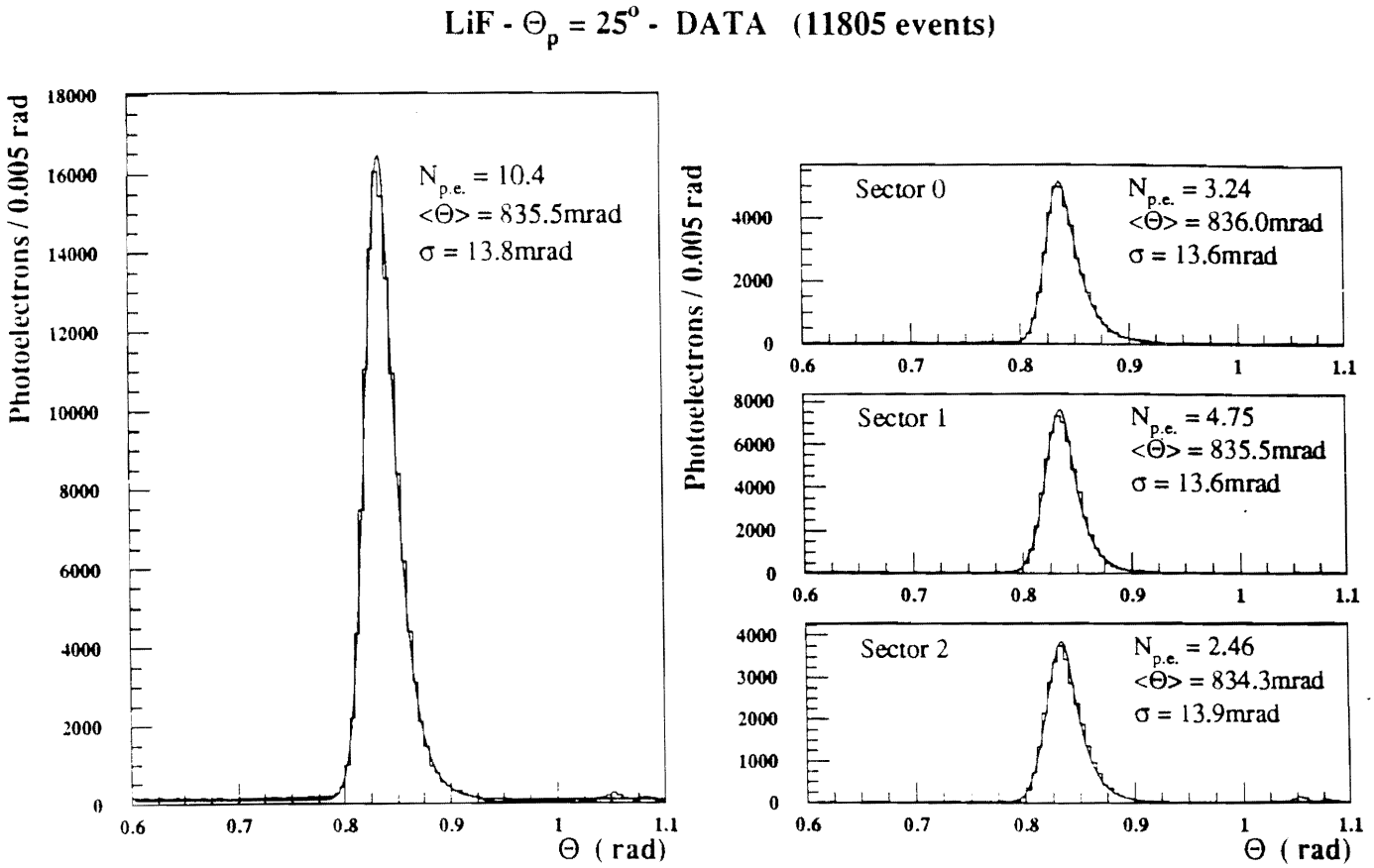

Fig. 20. The reconstructed Cherenkov θ angle from events of the preceeding figures, fit with <θ>=835.5 mrad, σ_θ=13.8 mrad/photon and a small background due to LiF scintillation [59].

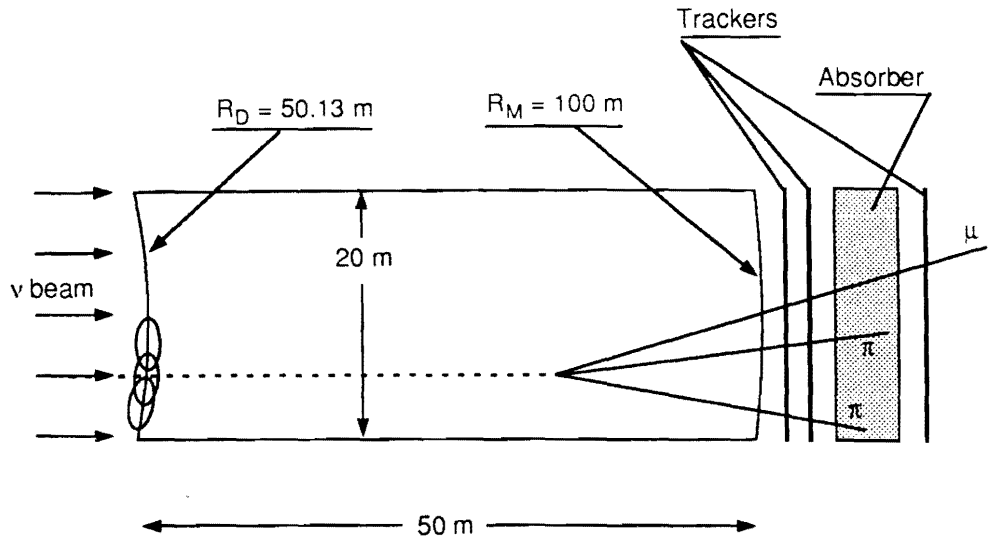

Fig. 21. A schematic view of a long baseline RICH radiator, mirror and detector along with an external tracker and muon filter.

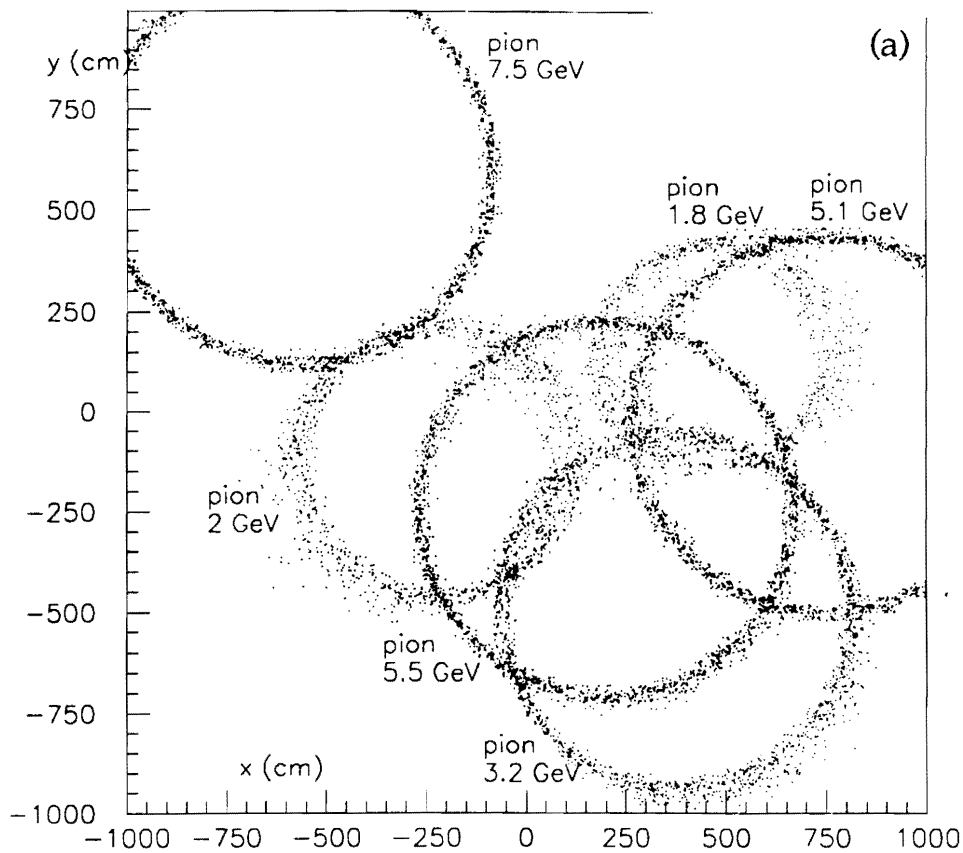

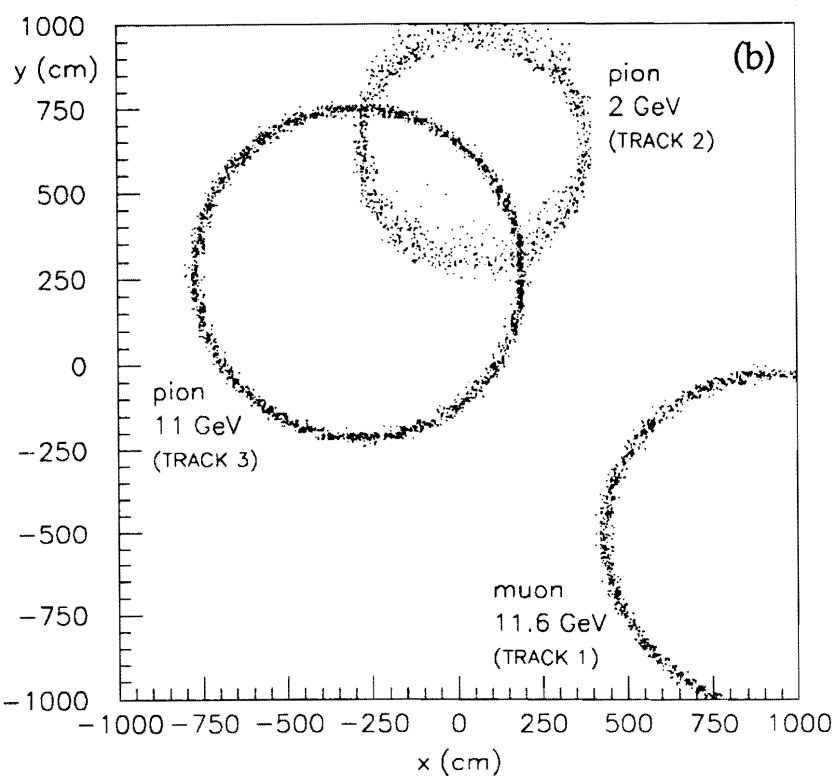

Fig. 22. Stereographic images for events with E_ν=40 GeV, z=25 m:

(a) $\nu_\tau X \to \tau^- \rho^0 \rho^0 \eta' \pi^+ p$, $\tau^- \to \nu_\tau \rho^- \to \nu_\tau \pi^- \pi^0$, $\rho^0 \to \pi^+ \pi^-$, $\eta' \to \pi^+ \pi^- \eta$, $\eta \to 3\pi^0$;

(b) $\nu_\mu p \to \mu^- \rho^+ \eta' \Delta^+ \pi^0$, $\rho^+ \to \pi^+ \pi^0$, $\Delta^+ \to \pi^+ \pi^0$, $\eta' \to \gamma \rho^0 \to \gamma \pi^+ \pi^-$.

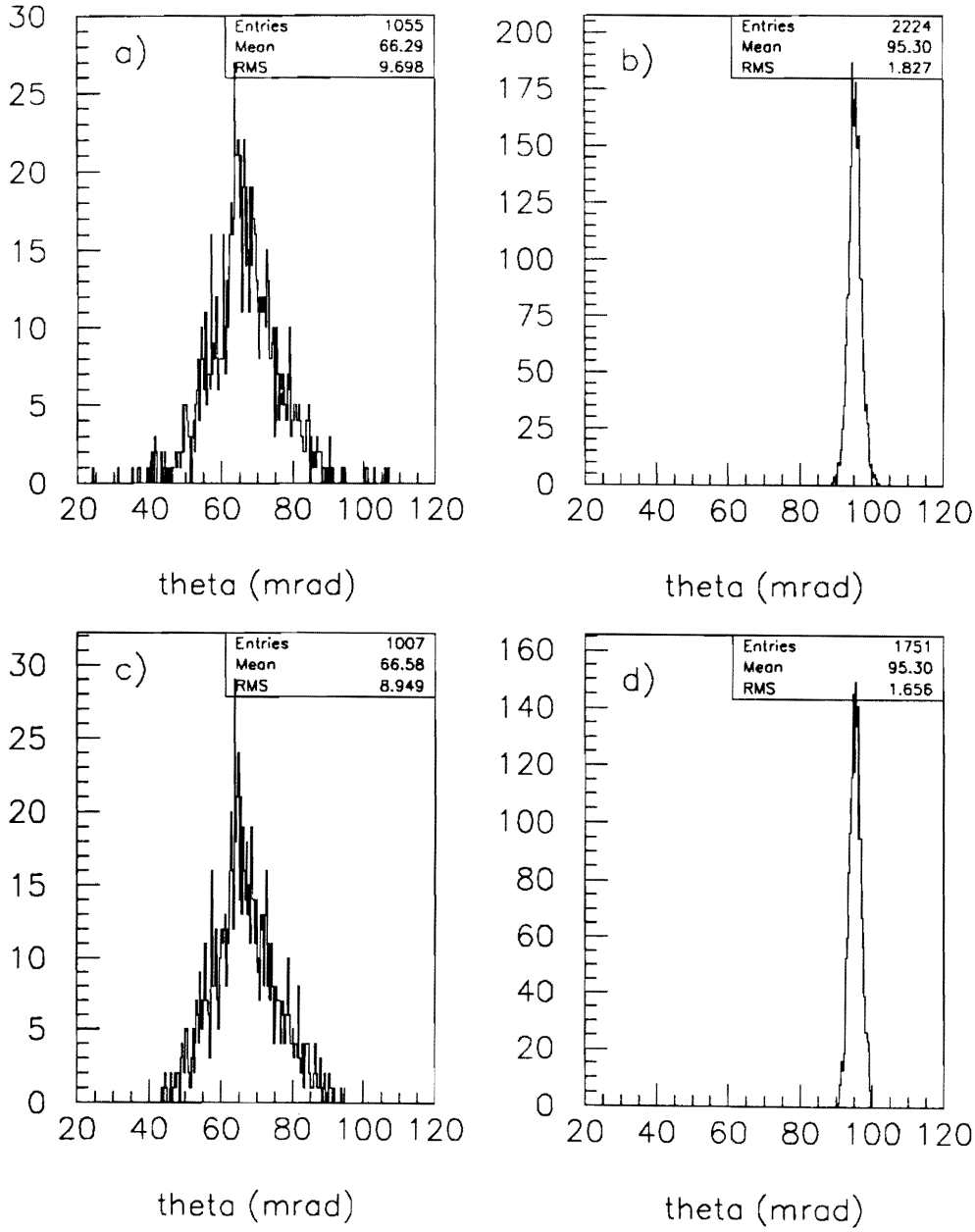

Fig. 23. Distributions of Cherenkov angle θ for tracks 2, 3 of Fig. 22b: **(a), (b)** generated; **(c), (d)** reconstructed.

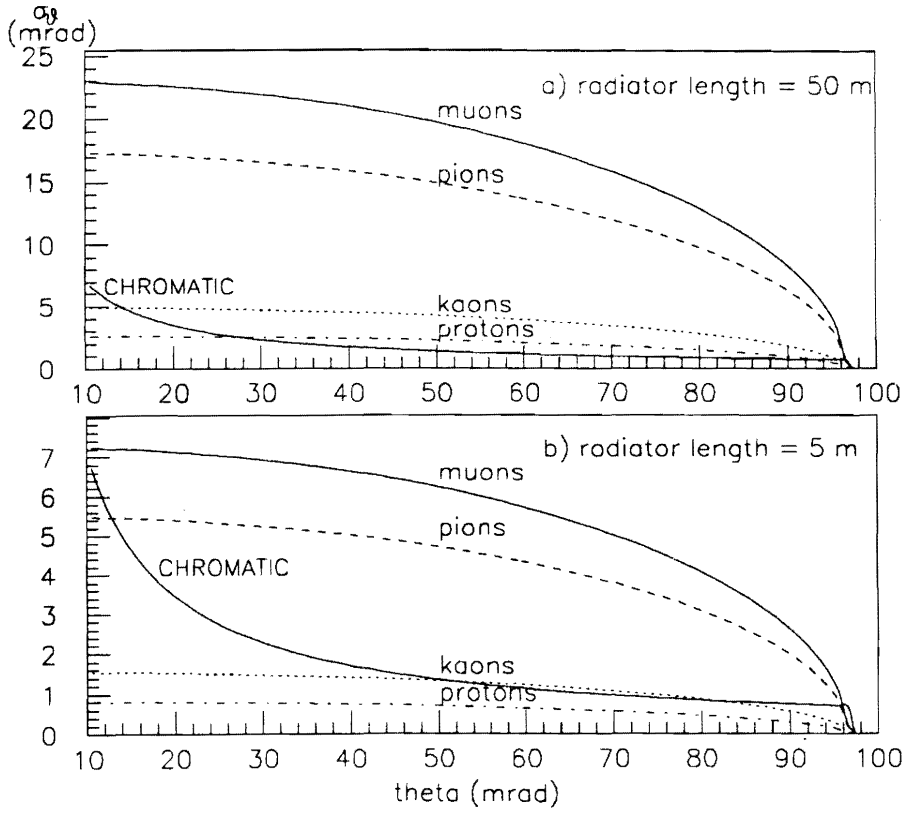

Fig. 24. The multiple scattering error σ_θ vs θ for μ, π, K, P with, for comparison, the UV chromatic error at <E>=6.7 eV, ΔE=0.8 eV: **(a)** for 50 m pathlength; **(b)** for 5 m pathlength.

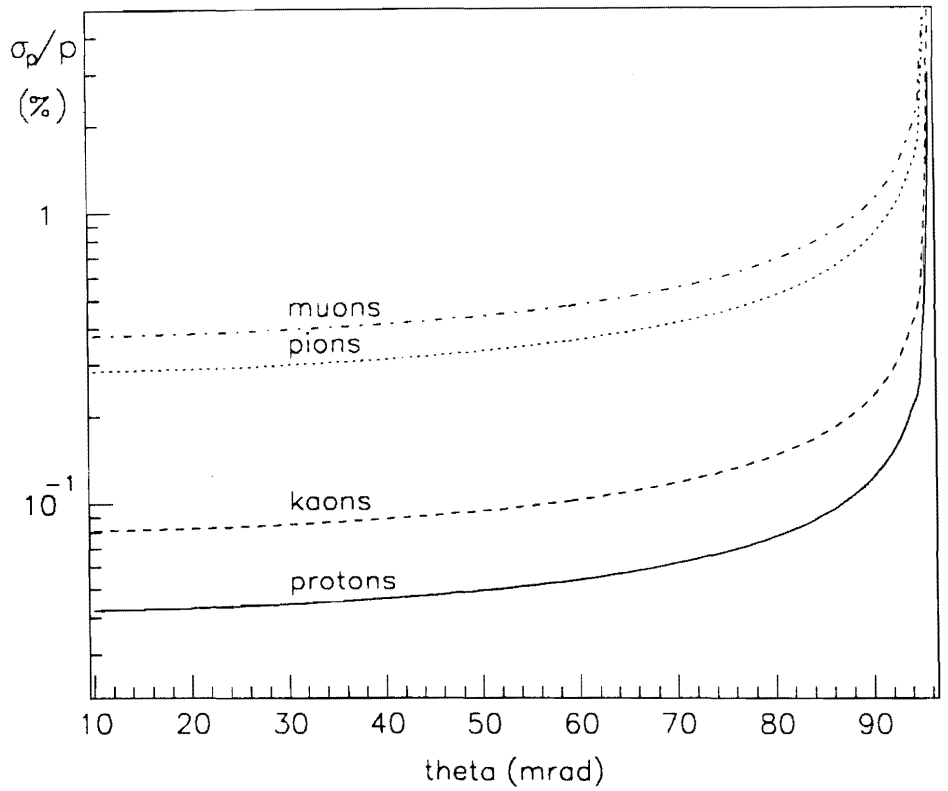

Fig. 25. The momentum resolution σ_p/p vs Cherenkov angle θ for μ, π, K, P assuming errors are from multiple scattering (Eq. 33).

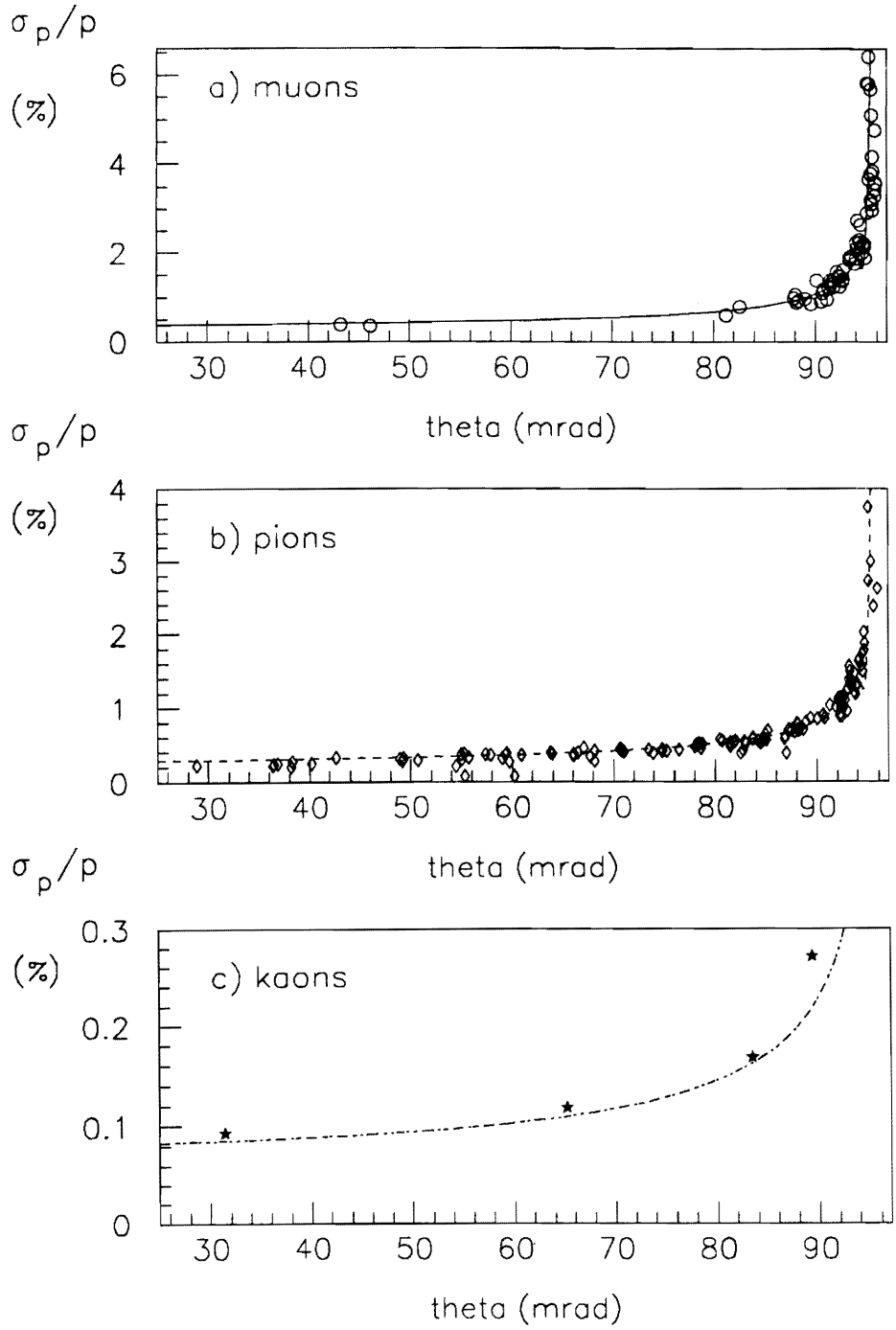

Fig. 26. Momentum resolution σ_p/p vs θ for all tracks from 209 CC νX events with measurement and multiple scattering errors, plotted for μ, π and Ks and compared to the MSD line of Eq. 33.

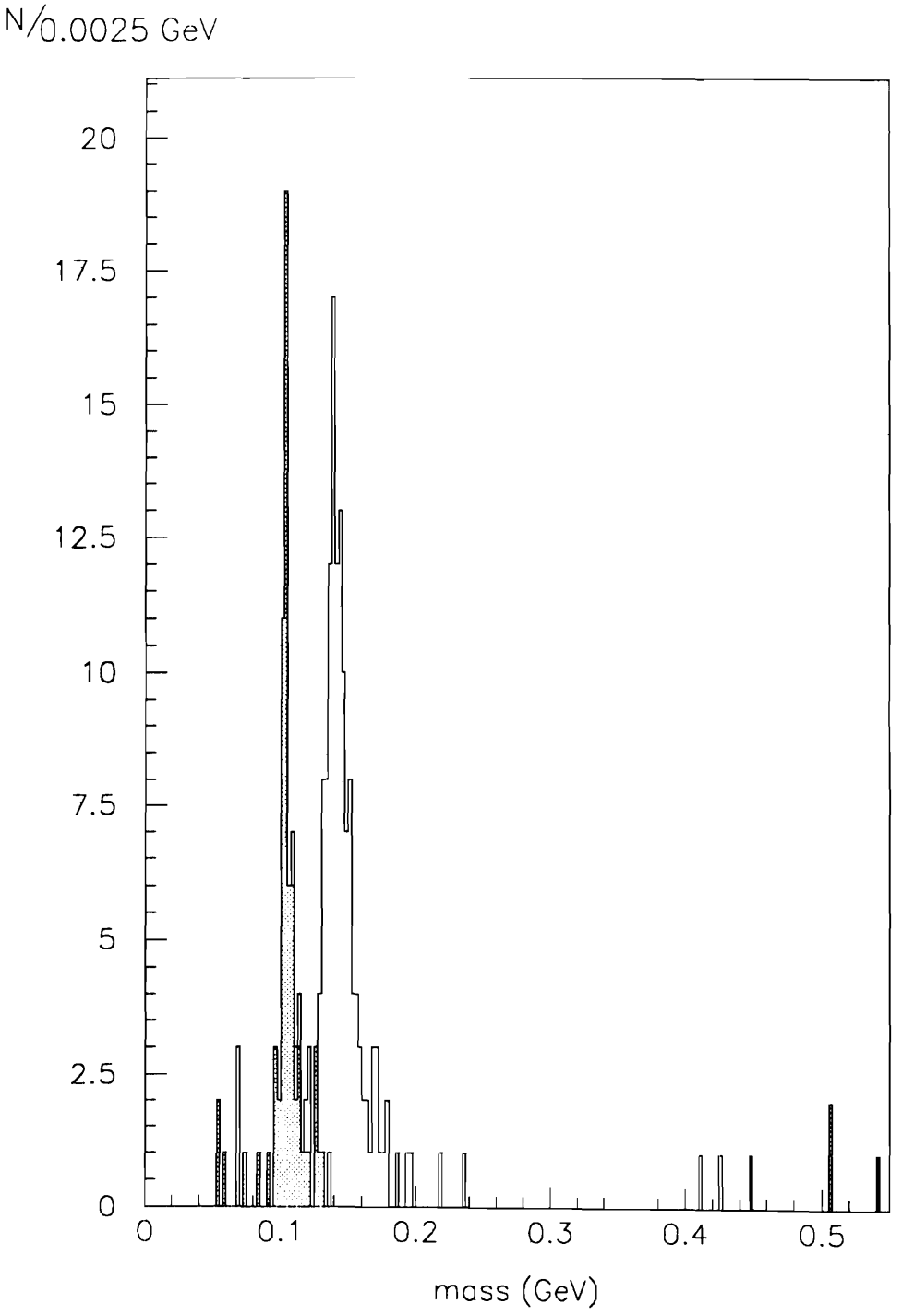

Fig. 27. The mass spectrum for the tracks of the preceeding figure. The mass was calculated via Eq. 34 from σ_θ, L and reconstructed θ. The μ, π and K tracks are grey, white and black, respectively.

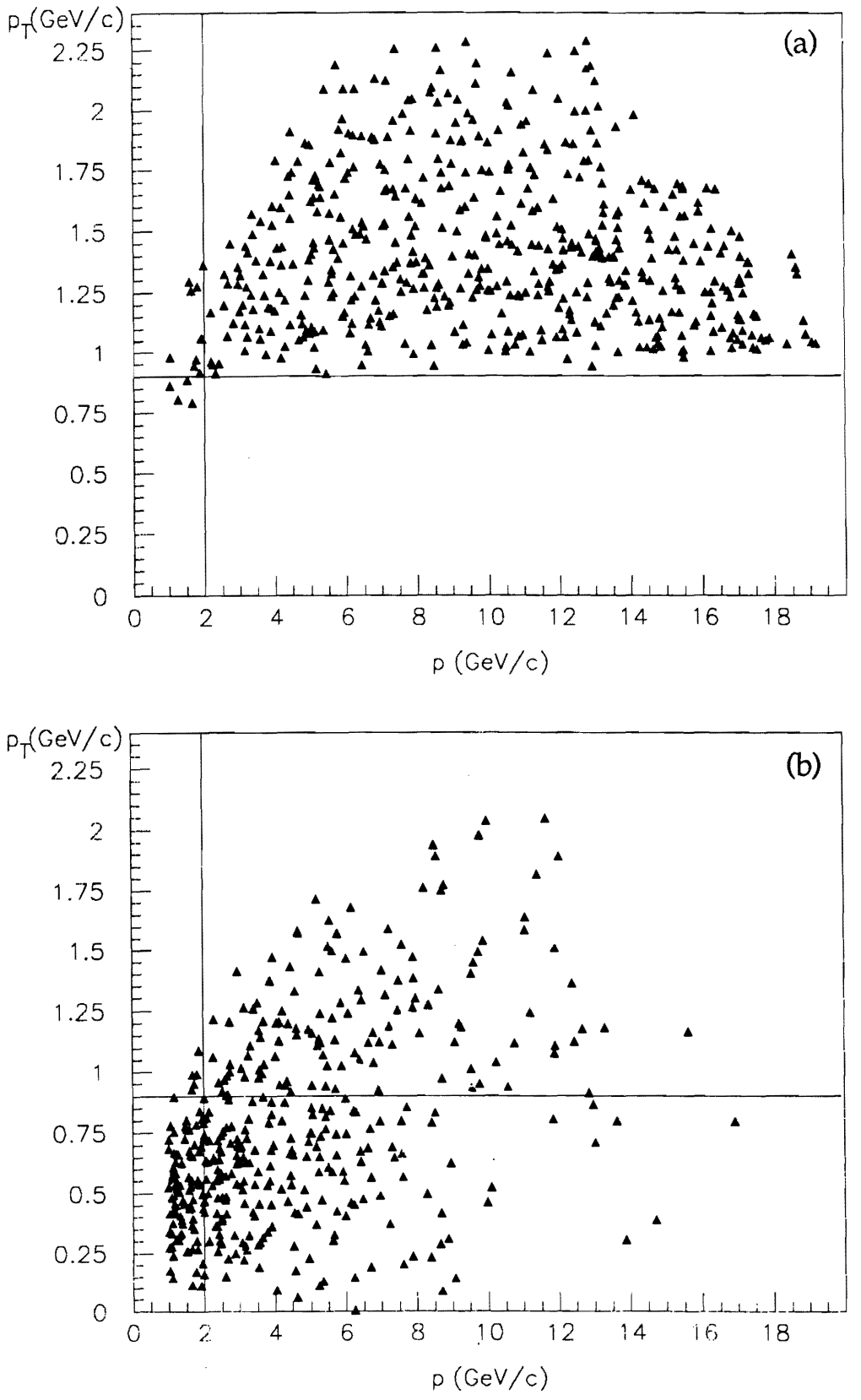

Fig. 28. Scatter plots of (p_t, p) for 500 CC events with E_ν=20 GeV: **(a)** $\nu_\mu p \rightarrow \mu X$ events; **(b)** $\nu_\tau p \rightarrow \tau X$, $\tau \rightarrow \mu X'$ events. The horizontal and vertical lines show selection cuts.